NUREG/CR-0746
UCRL-52624

THE EFFECTS OF TORUS WALL FLEXIBILITY ON FORCES IN THE MARK I BOILING WATER REACTOR PRESSURE SUPPRESSION SYSTEM--FINAL REPORT

S. C. Lu
G. S. Holman
E. W. McCauley

Prepared for
U. S. Nuclear Regulatory Commission
by
Lawrence Livermore Laboratory

NOTICE

Available from U. S. Nuclear Regulatory Commission Washington, D. C. 20555

Available from National Technical Information Service Springfield, Virginia 22161

NUREG/CR-0746
UCRL-52624

THE EFFECTS OF TORUS WALL FLEXIBILITY ON FORCES IN THE MARK I BOILING WATER REACTOR PRESSURE SUPPRESSION SYSTEM--FINAL REPORT

S. C. Lu
G. S. Holman
E. W. McCauley

Manuscript Submitted: October 1978
Date Published: October 1979

Prepared for

U.S. Nuclear Regulatory Commission
Washington, D. C. 20555
Under Interagency Agreement DOE 40-550-75
NRC FIN No. A 0203
by
Lawrence Livermore Laboratory
Livermore, CA 94550

operated by University of California

for the U.S. Department of Energy

FOREWORD

This report summarizes the FY78 results of a technical assistance program funded in FY77 and FY78 (B&R 2010 0402 FIN A 0203) by Engineering Branch, Division of Operating Reactors, Office of Nuclear Reactor Regulation, U.S. Nuclear Regulatory Commission. The program investigated the effects of wall flexibility on hydrodynamically induced loads in the torus-shaped pressure suppression chamber of a Mark I boiling water reactor.

Thanks are extended to Mike Gerhard of the Structural Mechanics Group for his work in generating the various finite element meshes that were used in the hydro/structure interaction analyses.

CONTENTS

LIST OF ILLUSTRATIONS

LIST OF TABLES

ABSTRACT

This report summarizes the FY78 results of a program funded in FY77 and FY78. The purpose was to investigate, through analytical models, the effects of wall flexibility on hydrodynamically induced loads in the torus-shaped pressure suppression chamber of a Mark I boiling water reactor, both in the event of a safety relief valve (SRV) discharge and a hypothetical loss-of-coolant accident (LOCA). Two-dimensional and three-dimensional analytical models for these two events were created by using the Monticello nuclear plant's geometry and finite element computer codes. Initial two-dimensional results were documented in the FY77 report (Lawrence Livermore Laboratory, UCRL-52506); those two-dimensional results are extended here by varying the pulse amplitudes and conducting nonlinear analyses for comparison with the linear analyses. Finally, three-dimensional analyses are conducted for the SRV discharge and LOCA chug problems. Our analytical models show that, compared to rigid wall response, flexibility in the torus shell significantly decreases hydrodynamic loads in the suppression chamber.

INTRODUCTION

The basic components of the Mark I boiling water reactor (BWR) containment system are a light-bulb-shaped reactor compartment (drywell) and a torus-shaped pressure suppression chamber (wetwell). The wetwell is partially filled with water and connected to the drywell by a series of large vent pipes. (See Fig. 1.) Working in conjunction with these basic components is the reactor pressure safety relief valve (SRV) system, which consists of piping, discrete from the large vent pipes, leading from the relief valves and terminating near the bottom of the wetwell pool. (See Fig. 2.)

In the case of a hypothetical loss-of-coolant accident (LOCA)--an event that has never happened in a BWR--air followed by steam is injected into the wetwell through the large vent system. In the case of a safety relief discharge, a normally occurring phenomenon in the BWR operation, air and steam released by the relief valves are transmitted by the SRV piping to the bottom of the wetwell pool. In either of these events, potentially damaging pressure buildup in the primary containment is prevented as the steam discharged into the wetwell pool is harmlessly condensed.

The air and steam forced into the water pool induce hydrodynamic loads on both the vent system and the torus shell. The ability of these structures to sustain the induced loads is fundamentally important to the containment system's functioning either during a LOCA or an SRV discharge.

Determining the characteristics of the hydrodynamic loads is the first step toward evaluating the containment design's strength. For example, a test program was conducted for the NRC that used a 1/5-scale model of a Mark I containment system to investigate the hydrodynamic loads resulting from a hypothetical LOCA.[1,2] That 1/5-scale test model, like experimental models used by the Mark I Owner's Group, was designed with a relatively thick torus wall to facilitate isolating the hydrodynamics. However, the disproportionate shell thicknesses of the various test models introduce significant wall

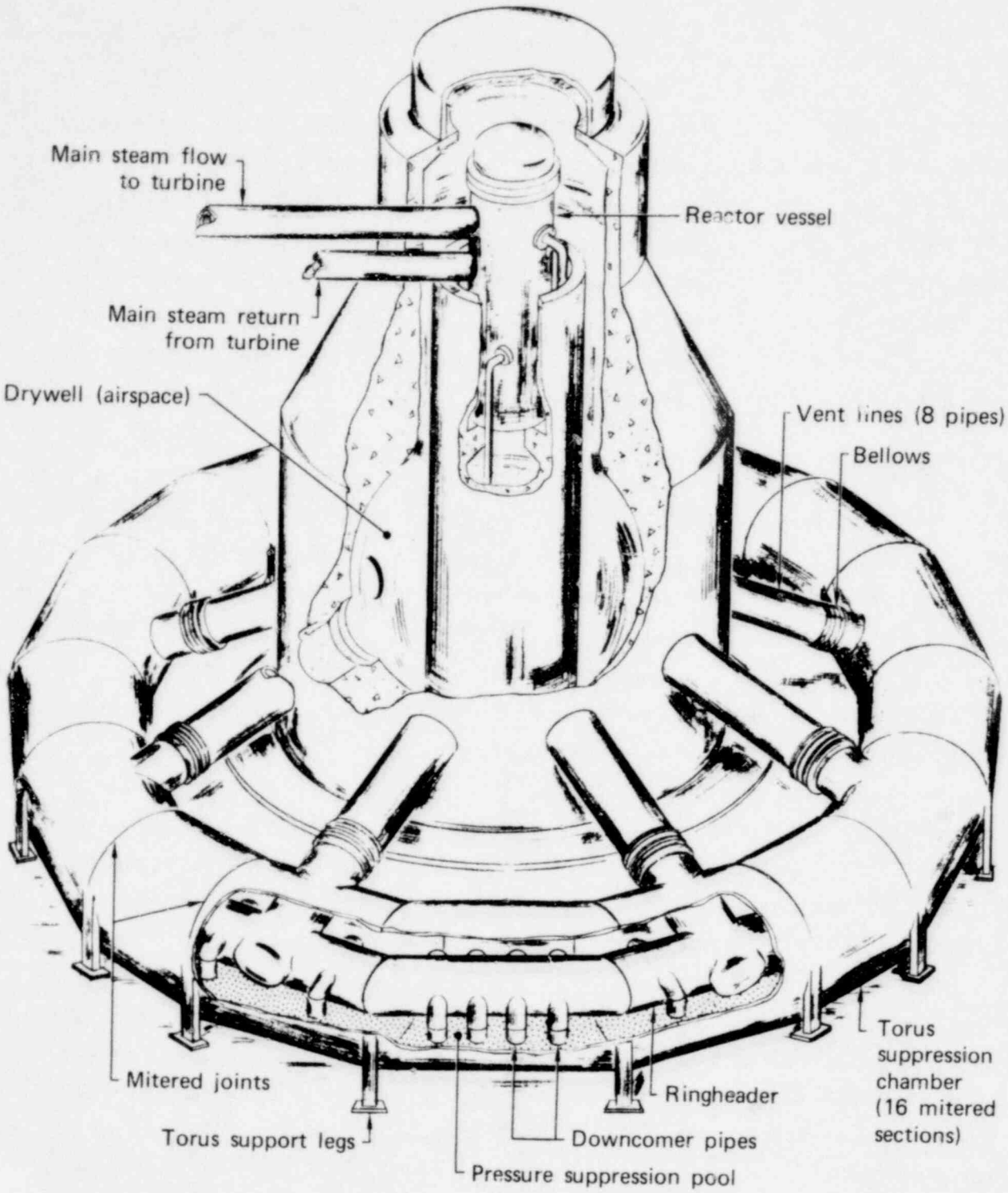

FIG. 1. Artist's rendering of a Mark I boiling water reactor, showing the essential elements of the pressure suppression system.

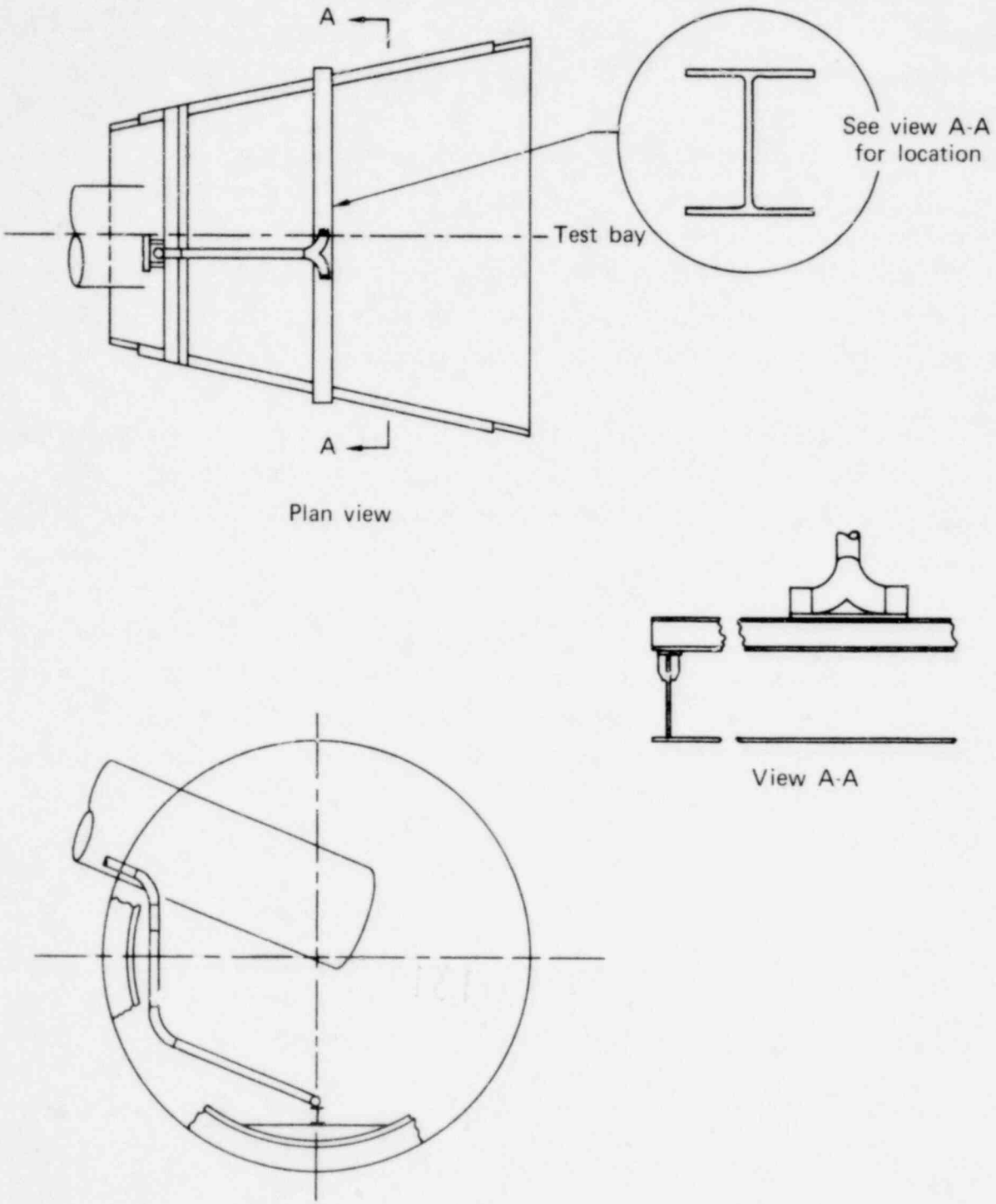

FIG. 2. Location of safety relief valve (SRV) discharge line and support structures.

stiffness that does not exist in real containment structures, and, inasmuch as real shells are flexible, the forces measured in these rigid test models may not correspond with forces in real containment structures. Study is therefore required so that the hydrodynamic loads of rigid-walled test models can be properly applied to full-scale flexible-walled structures.

This report describes an analytical program that investigates, in a qualitative sense, the influence torus wall flexibility has both on hydrodynamically induced pressure within the torus and on the resultant force at the torus shell surface. The degree of wall flexibility is characterized by the torus minor-diameter-to-shell-thickness ratio, which is varied from 0 (perfectly rigid) to 600 (nominal plant geometry).

Three problems are of interest. The first is an analysis of air/steam forces in an SRV discharge. The other two are studies of forces in the early and late stages of a LOCA--the phenomena of LOCA downcomer clearing and LOCA chugging, respectively.

The analytical program, initiated in FY77, is based on the geometry of the Monticello BWR power plant operated by the Northern States Power Company of Minnesota. Part I of this work was issued to present FY77 results.[3] This report summarizes the final results of FY78.

SRV-INDUCED HYDRO/STRUCTURE INTERACTION

During normal BWR operation, steam is periodically discharged to the suppression pool through safety relief valves to maintain reactor pressure within design operating limits. As shown in Fig. 2, each SRV line from the reactor vessel terminates at a discharge header located near the bottom of the suppression pool.

The two-dimensional finite element mesh developed in FY77 to model the SRV discharge problem (Fig. 3) represents an idealized plane section taken at a right angle through the wetwell torus. No motion is allowed at the shell waist, a reasonable boundary condition considering the torus support structures. The discharge of noncondensable air forced ahead of the steam flow is modeled by a single air bubble located at the exit of the discharge pipe. The inner surface of the bubble is loaded by a theoretical pressure pulse, derived using Rayleigh bubble arguments,[4] which has a peak overpressure of 10.4 bars and a duration of 40 ms.

Linear finite element analyses of this model, conducted in FY77 using the finite element code DTVIS2[5] (see Appendix for description) for shell D/t ratios of 0, 100, 300, and 600 concluded:

- Increasing shell flexibility decreases the maximum pressure seen by the torus wall.
- Total vertical load on the torus shell diminishes with increasing wall flexibility.

In FY78, the two-dimensional linear analyses were extended to include a pulse variation study and a limited investigation of nonlinear effects. In addition, the severe modeling constraints implicit in the two-dimensional modeling of the three-dimensional system were removed by a comprehensive series of three-dimensional calculations. These results, while still qualitative, provide a much improved basis for understanding the expected effects in real structures.

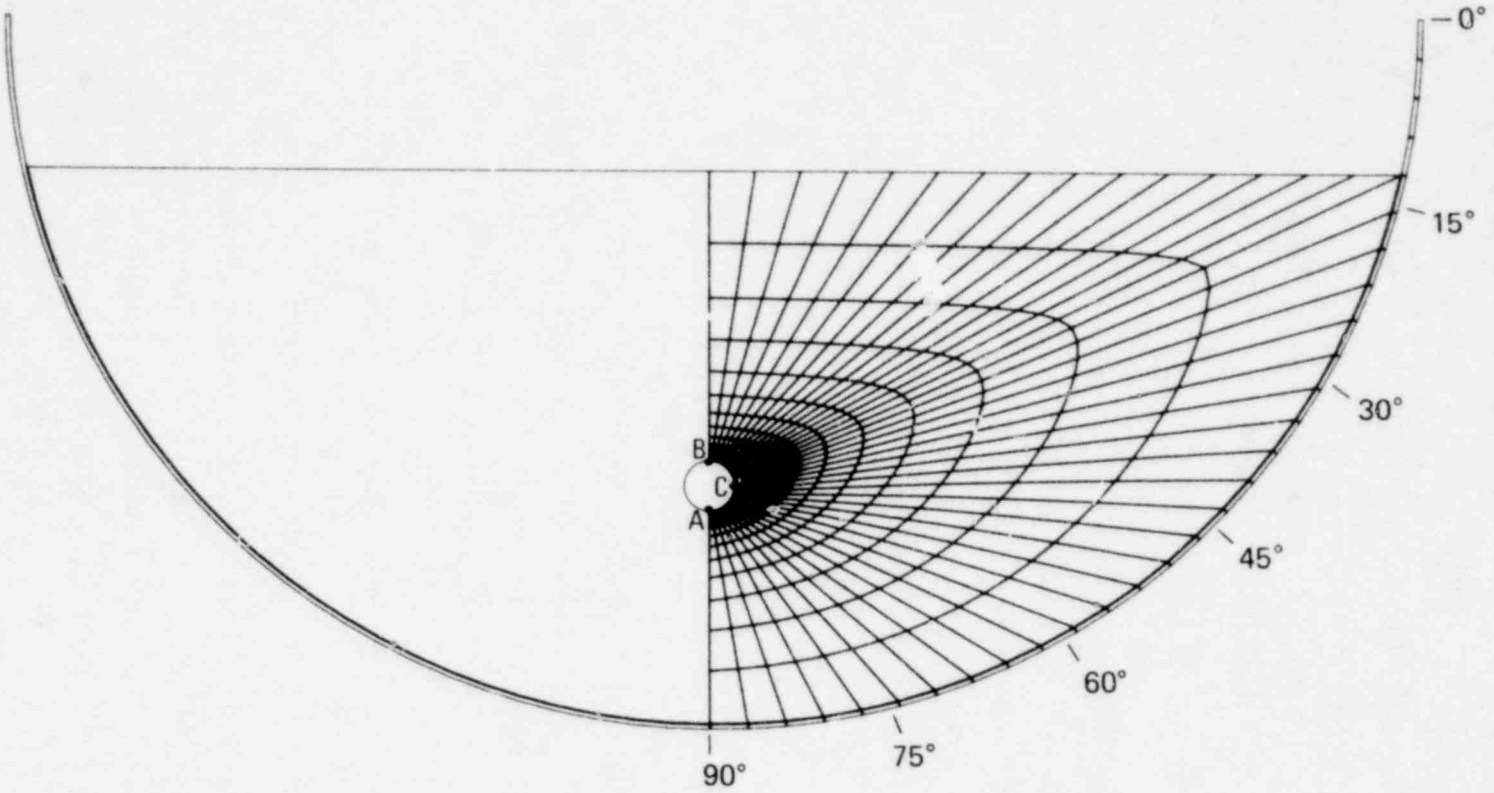

FIG. 3. Typical finite element mesh for the two-dimensional SRV discharge problem (D/t = 300).

TWO-DIMENSIONAL PULSE VARIATION STUDY

The pulse variation study confirmed previous conclusions from the FY77 analyses and extended the data base for a wider range of pulse amplitudes and rise times. The general shape and total impulse of the pressure pulse were held unchanged, but pulse amplitude was increased or decreased by 30%, as shown in Fig. 4.

Numerical results were generated by the linear finite element computer code DTVIS2[5] for D/t values of 0, 100, 300, and 600. The computed pressure histories at the wetwell pool bottom and the total vertical force acting on the torus shell for the case of +30% pulse amplitude are depicted respectively by Figs. 5 and 6, and by Figs. 7 and 8 for the case of -30% pulse amplitude. The effect of torus wall flexibility for different pulse amplitudes (on the pool bottom peak pressure and on the peak vertical force) is characterized by the sensitivity curves shown in Figs. 9 and 10. Peak pressures are normalized with respect to the peak input of the basic pulse (10.4 bars), whereas peak vertical forces are normalized with respect to that calculated for the rigid shell subjected to the basic pulse.

TWO-DIMENSIONAL NONLINEAR ANALYSIS

Because of the relatively large fluid deformation observed in the two-dimensional linear analysis, the significance of nonlinear effects was assessed. A two-dimensional nonlinear finite element code NIKE2D[6] (formerly NSAP2D; see Appendix for description) was used to generate numerical results. The basic problem used in the analysis has a D/t ratio of 600 and uses the nominal input bubble pressure pulse.

Both linear and nonlinear results are generated for comparison. In the NIKE2D code, the linear results are achieved by scaling down the input pulse amplitude by a load factor of 0.01, which virtually eliminates all nonlinear effects. The final solution is then scaled up by a factor of 100 to obtain the desired linear results.

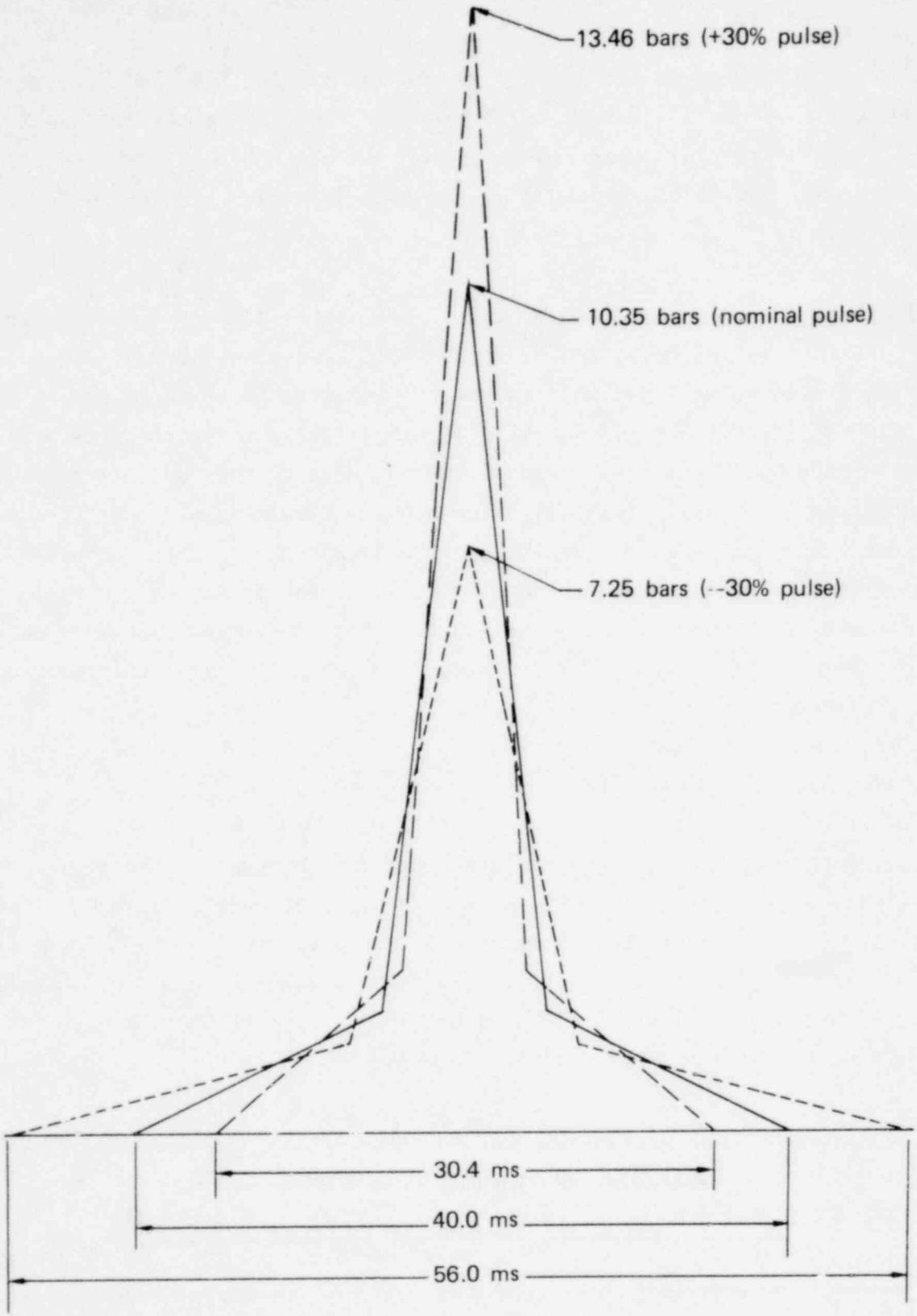

FIG. 4. Variation of SRV pulses.

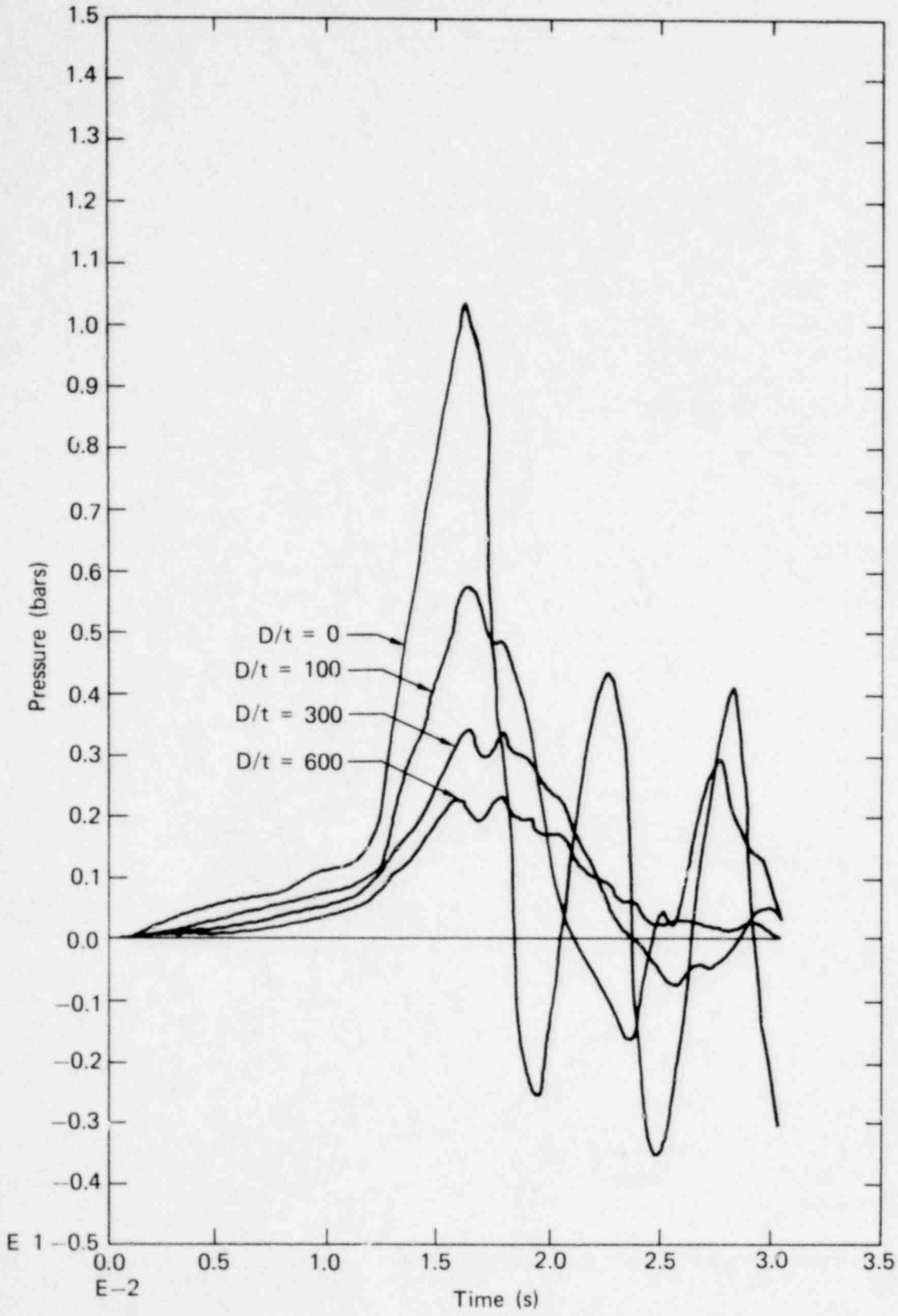

FIG. 5. Effect of torus shell thickness on pool bottom pressure history (SRV +30% pulse).

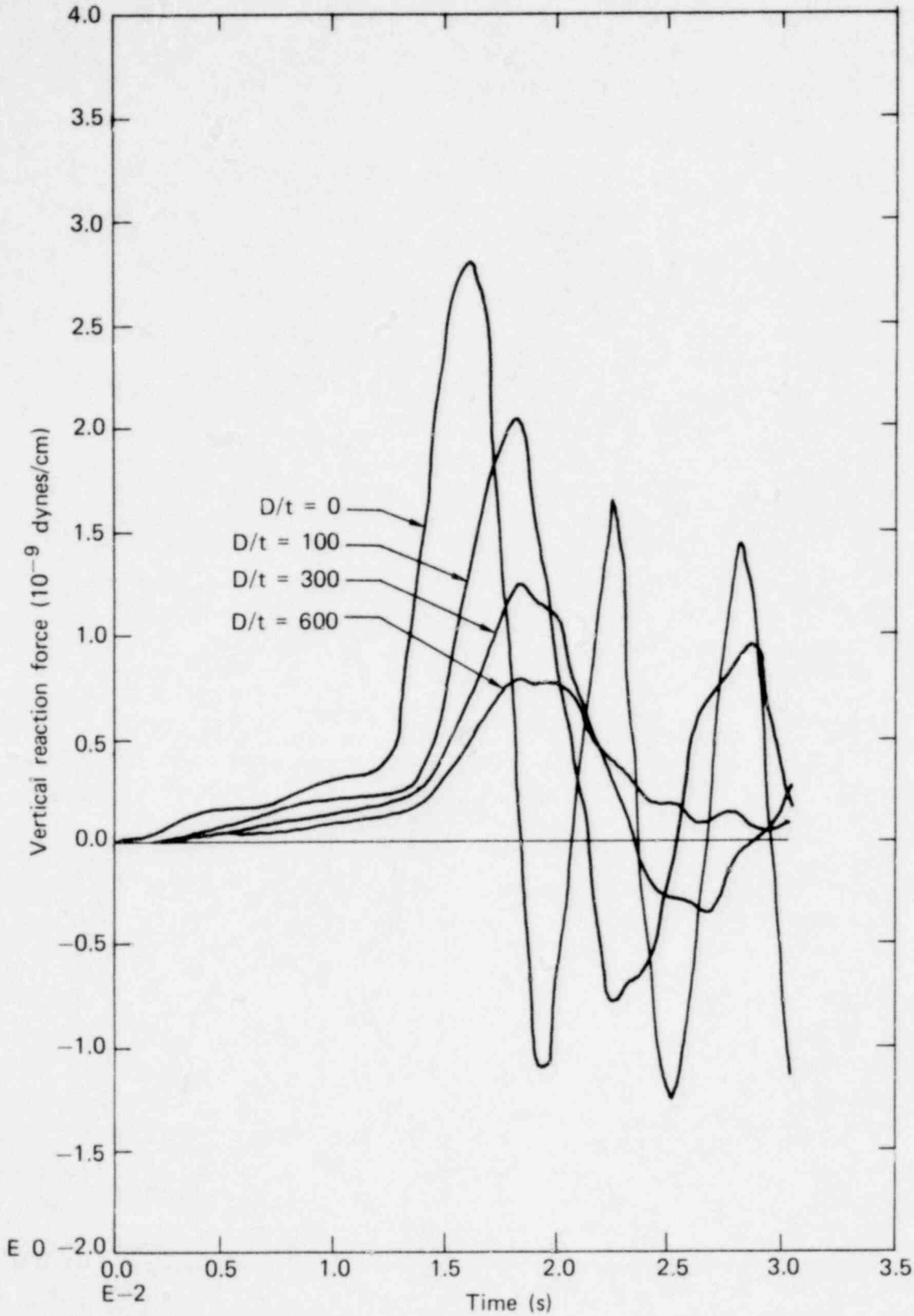

FIG. 6. Effect of torus shell thickness on total vertical force (SRV +30% pulse).

1317 237

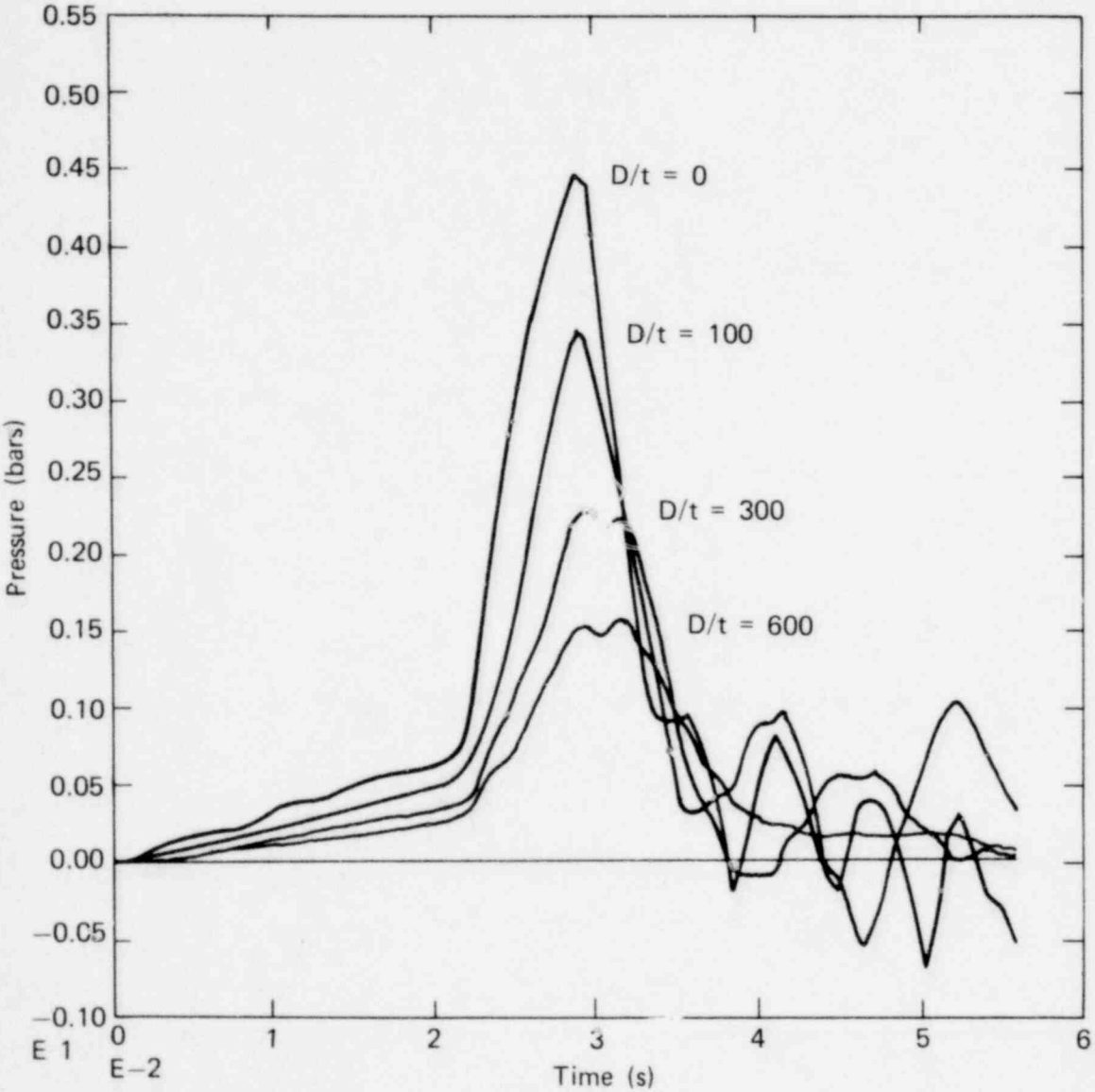

FIG. 7. Effect of torus shell thickness on pool bottom pressure history (SRV -30% pulse).

1317 234

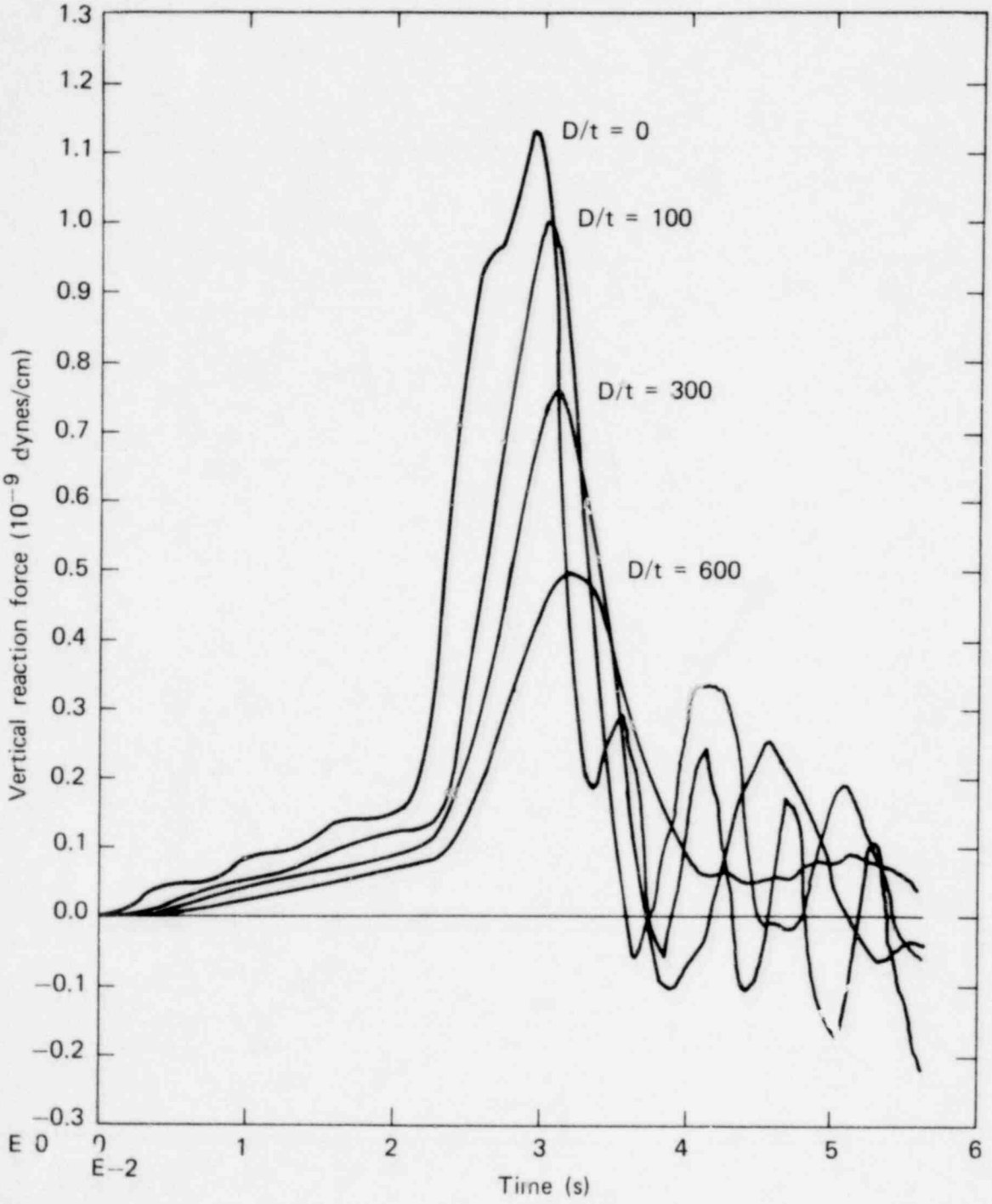

FIG. 8. Effect of torus shell thickness on total vertical force (SRV -30% pulse).

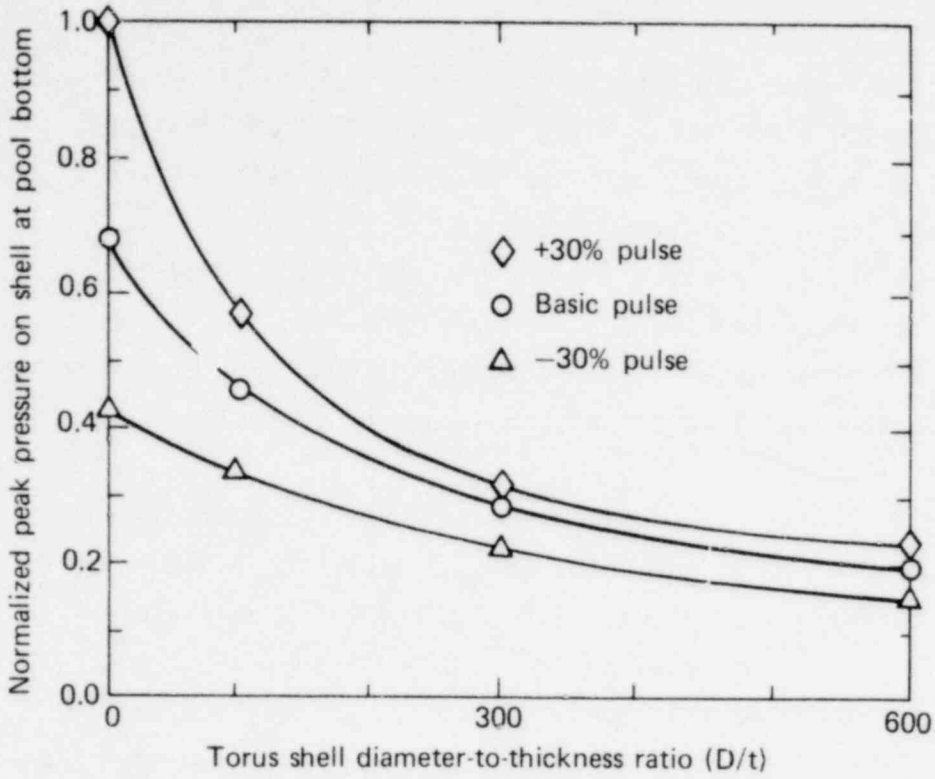

FIG. 9. Effect of torus shell thickness on normalized peak overpressure (SRV discharge).

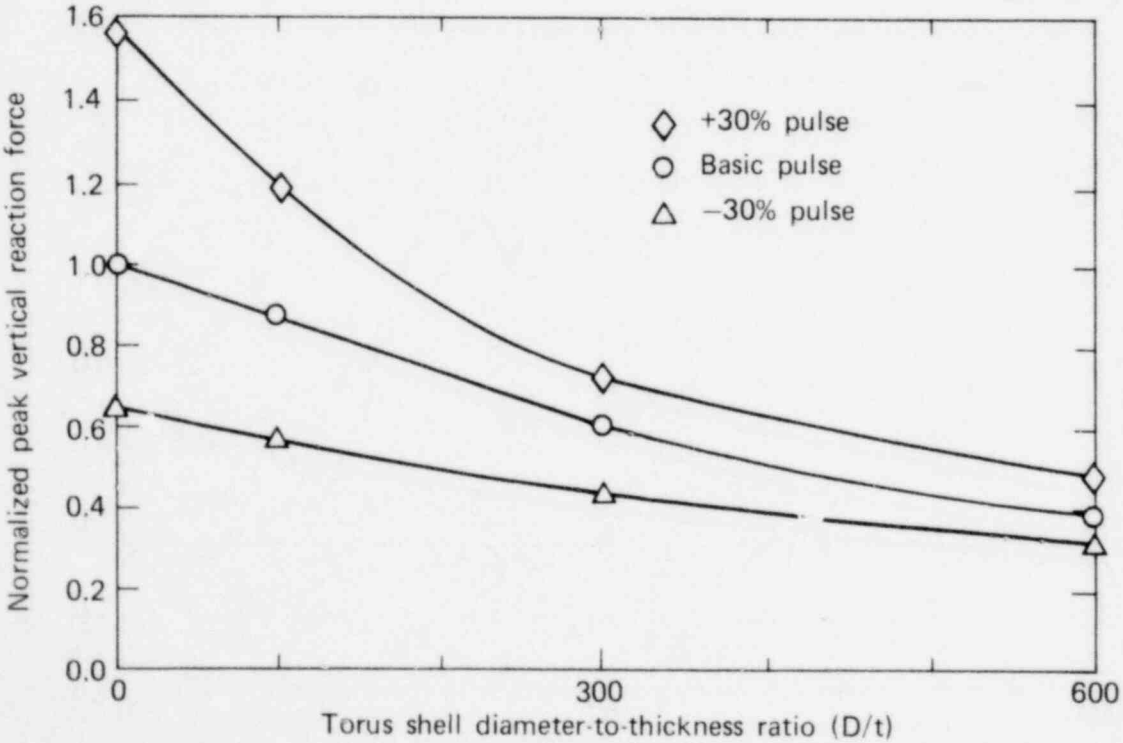

FIG. 10. Effect of torus shell thickness on normalized peak vertical reaction force (SRV discharge).

The linear and nonlinear comparison is depicted in Fig. 11, which shows the pool bottom pressure histories. It is seen that the nonlinear peak pressure is about 15% higher than the linear result. The nonlinear effect is therefore considered small for the following reasons:

- Only qualitative results are of interest in the idealized two-dimensional approach.
- There are other uncertainties; approximations resulting from model idealization and load definition, among other factors.

Nonlinear NIKE2D results were not compared directly with the linear DTVIS2 results since the two codes use different types of finite elements to represent the thin-shell structure; i.e., thin-shell elements by DTVIS2 and 8-node quadrilateral elements by NIKE2D. Although the thin-shell element is a better choice for modeling thin-shell structures, it was not available in our version of NIKE2D. As shown in Fig. 12, the quadrilateral element tends to produce higher peak pressue than the thin element. Again, the small difference is not considered significant.

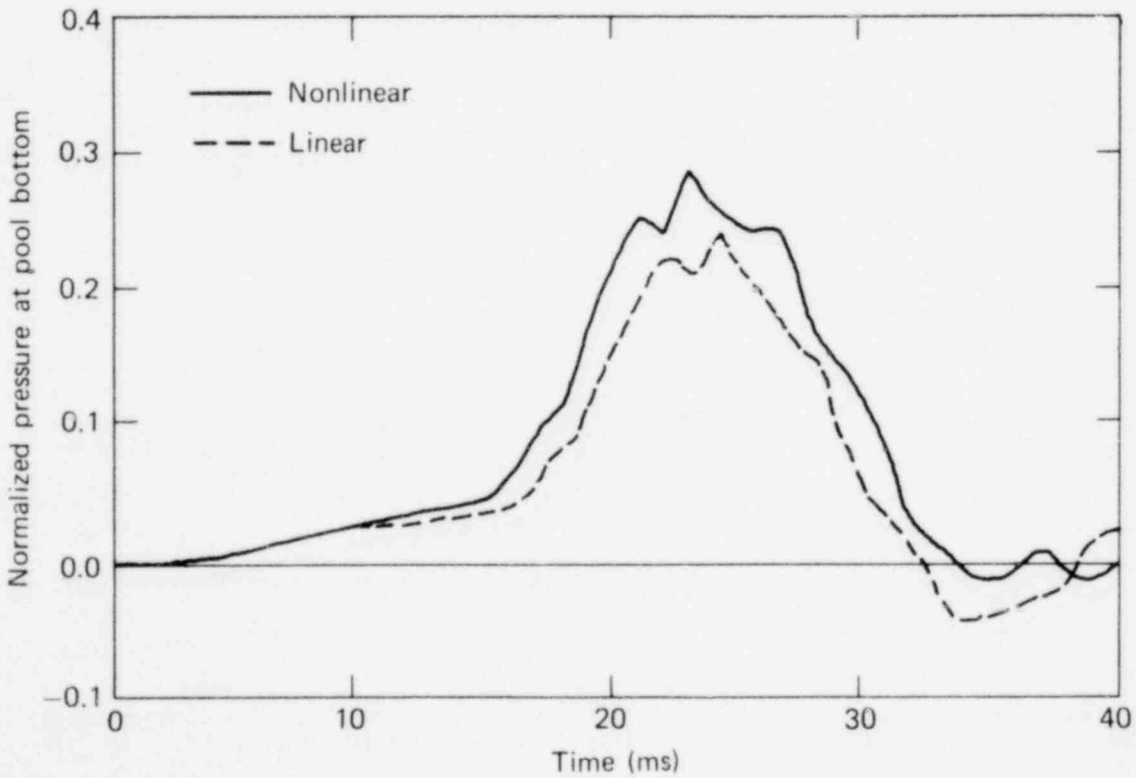

FIG. 11. Comparison of NIKE2D linear and nonlinear SRV analyses (plane-strain analysis, D/t = 600).

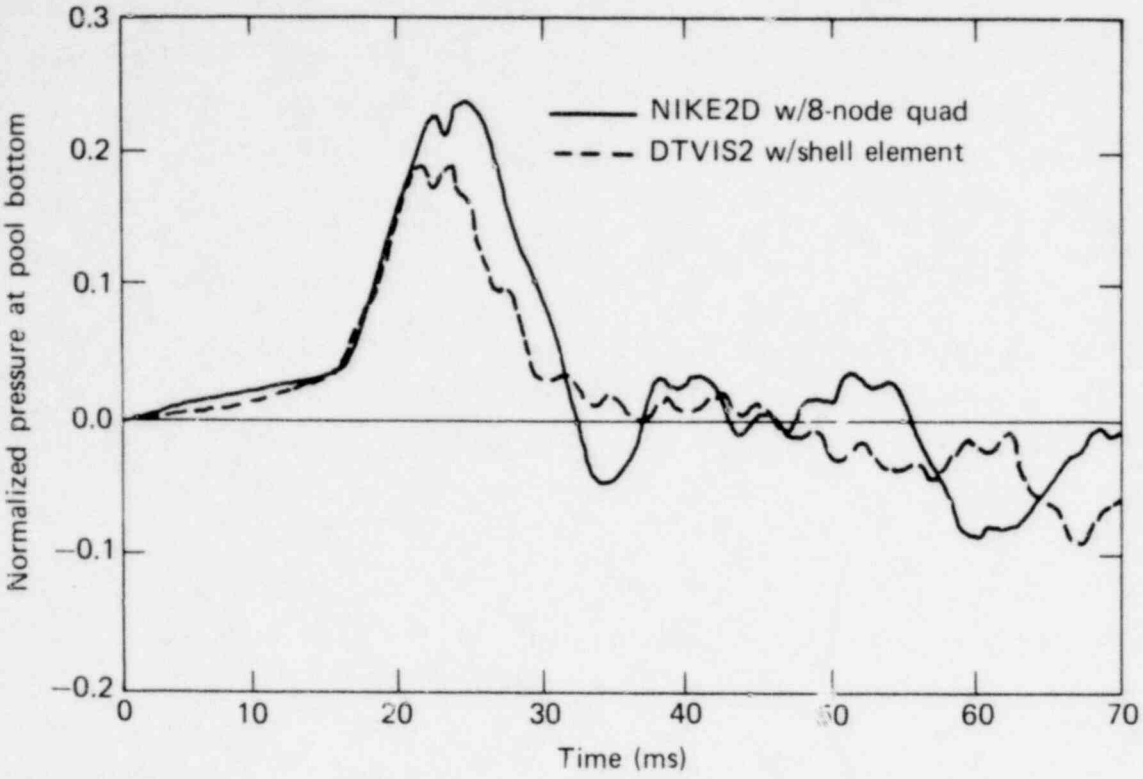

FIG. 12. Comparison of DTVIS2 and NIKE2D linear SRV analyses (D/t = 600).

THREE-DIMENSIONAL INVESTIGATIONS

The result of the two-dimensional analyses indicate, in a qualitative sense, that increasing shell wall flexibility will decrease the maximum pressures seen at the torus wall. However, quantifying the magnitude of the reduction is beyond the capabilities of the simple planar model. Consider, for example, that the "bubble" in the two-dimensional model really represents a cylindrical source of infinite extent, implying an unrealistically large energy input to the problem. Furthermore, the two-dimensional model is incapable of treating bending in the shell outside the plane of the bubble. Therefore, it was considered important to conduct three-dimensional analyses of the torus under SRV loading to determine the effect of the true torus geometry on hydrodynamic loading in the suppression pool.

A series of three-dimensional analyses of one torus bay was completed for shell D/t ratios of 0, 300, and 600 using the finite element code

SAP4 (see Appendix). To make a comparison of results between the two- and three-dimensional SRV analyses more meaningful, an initial series of three-dimensional analyses simulated the two-dimensional DTVIS2 mesh.

Three-Dimensional Plane-Strain Analyses

To provide an intermediate link between the two- and three-dimensional SRV analyses, the two-dimensional DTVIS2 finite element mesh was expanded to three dimensions and analyzed with SAP4. Three problems were run with this new "slab" mesh, corresponding to the DTVIS2 analyses, for shell D/t ratios of 0, 300, and 600.

Initially a three-element thickness was defined for the slab mesh, but this was reduced to a one-element layer after a comparison study (using D/t = 300) indicated a one-element layer was sufficient to characterize the plane-strain problem. The current slab problem (Fig. 13) uses 1208 nodal points to define a total of 545 three-dimensional fluid elements (including 25 "zero shear" slip elements) and 29 two-dimensional thin-shell elements.

The water is modeled as a nearly incompressible elastic material. A trace shear modulus (approximately six orders of magnitude less than the bulk modulus) is included to stabilize the problem. To prevent "locking" of the mesh in the problem, the bulk and shear terms in the water are integrated separately using one- and two-point quadrature, respectively.[4,8]

The first comparison between two- and three-dimensional plane-strain analyses (using D/t = 300) indicated excellent agreement in both nodal displacements (Fig. 14) and pressures (Fig. 15) predicted at the pool bottom, agreement that was consistently repeated between both models at other locations as well. It is of interest to note that the pressure history in the finite element directly beneath the bubble follows the nominal input pulse somewhat more closely in the two-dimensional model (Fig. 16) than in the three-dimensional slab (Fig. 17), indicating that the 1.0 ms time step used in the three-dimensional analysis is perhaps too coarse. Repeating the calculation with a 0.5 ms time step showed that this indeed was the case (see Fig. 18).

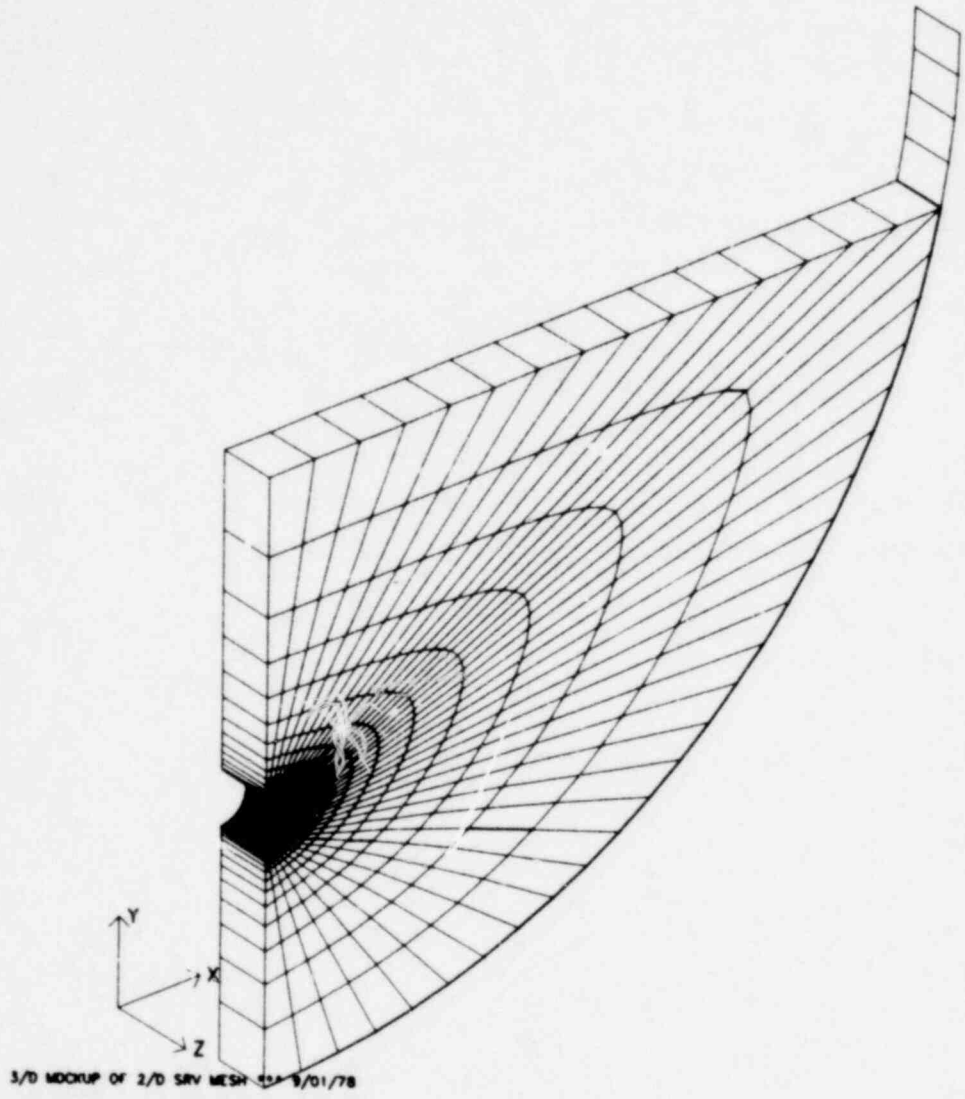

FIG. 13. Three-dimensional slab representation of the DTVIS2 two-dimensional SRV finite element mesh.

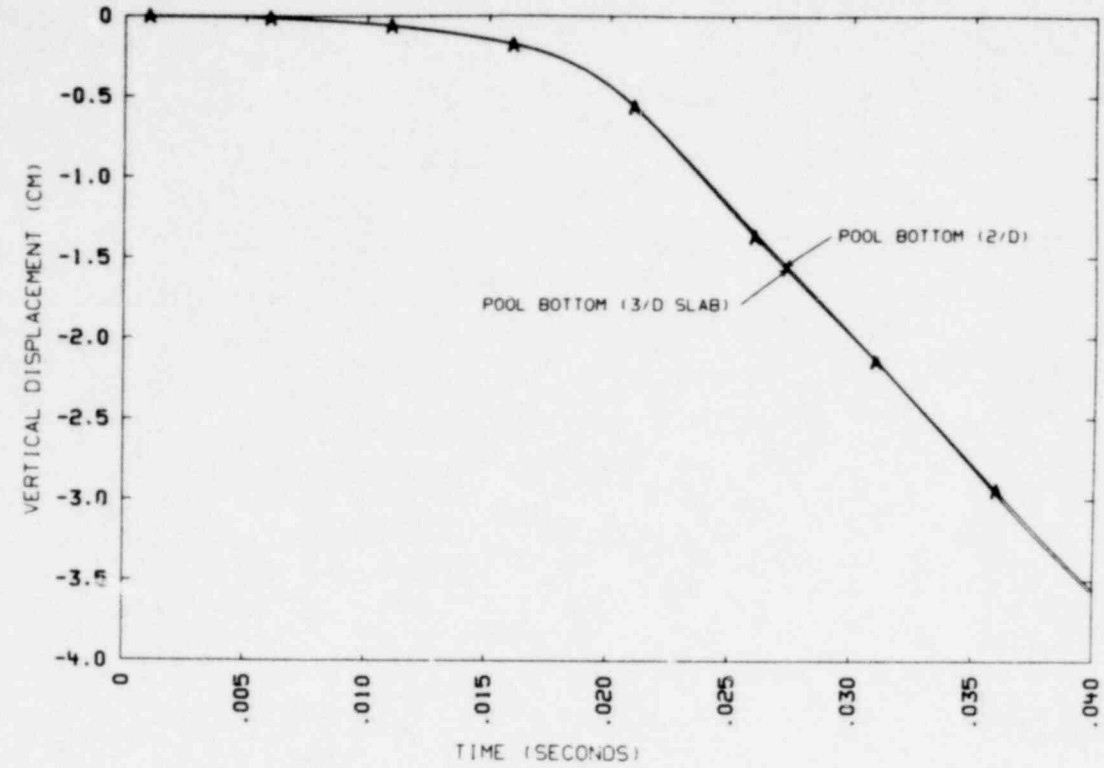

FIG. 14. Comparison of vertical displacement at pool bottom predicted by two- and three-dimensional plane-strain analyses (D/t = 300).

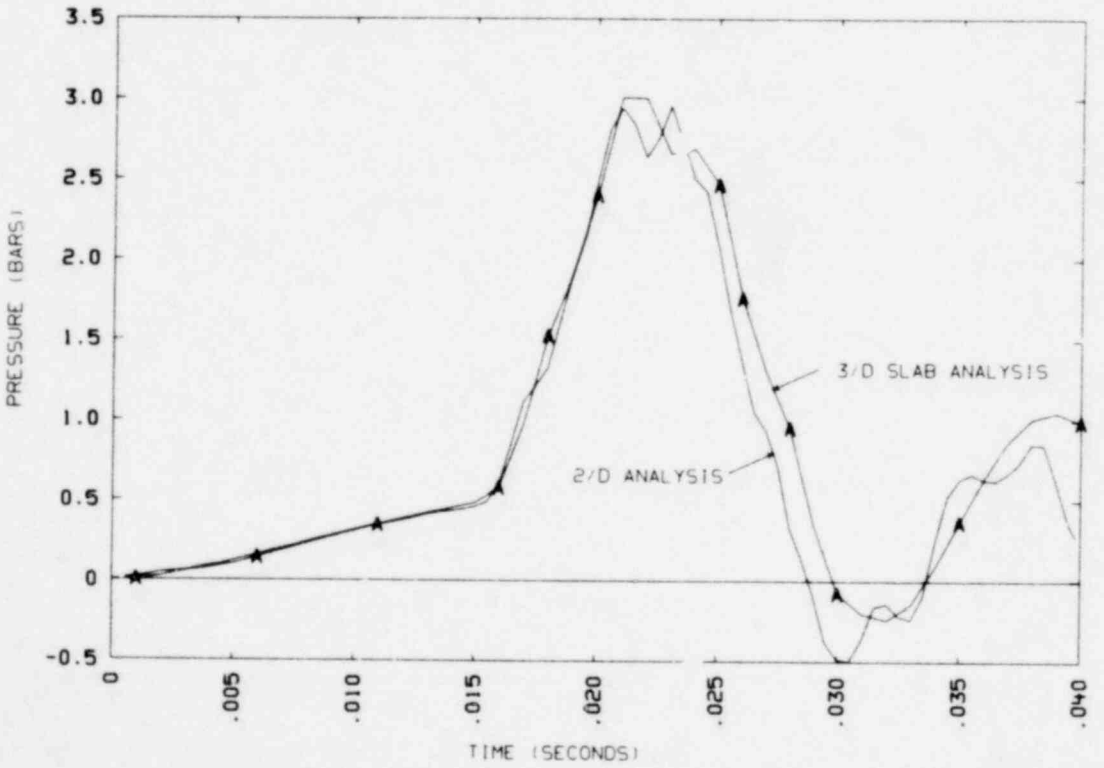

FIG. 15. Comparison of pressure response at pool bottom predicted by two- and three-dimensional plane-strain analyses (D/t = 300).

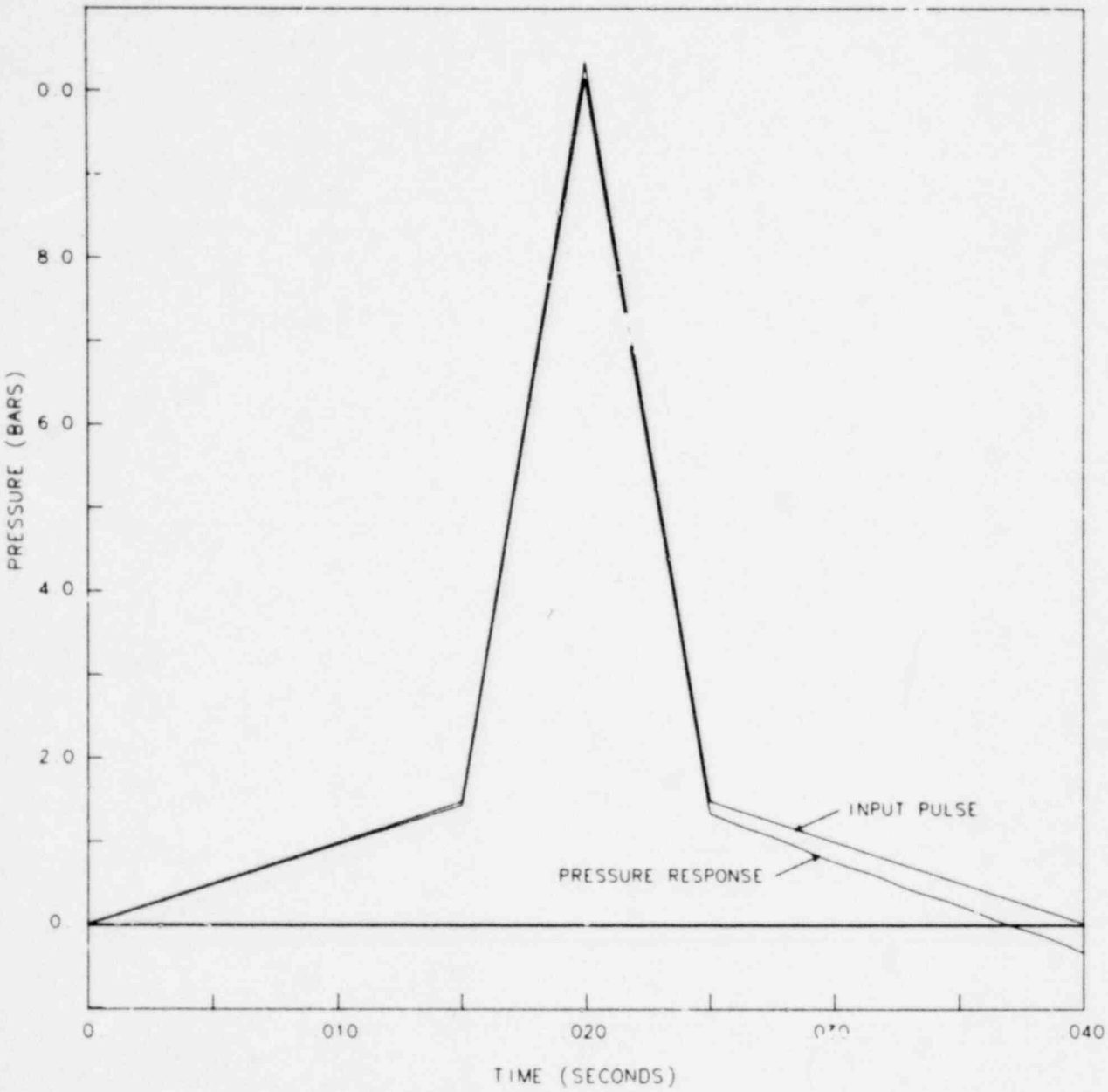

FIG. 16. Pressure response at bottom of bubble (two-dimensional, dt = 0.5 ms).

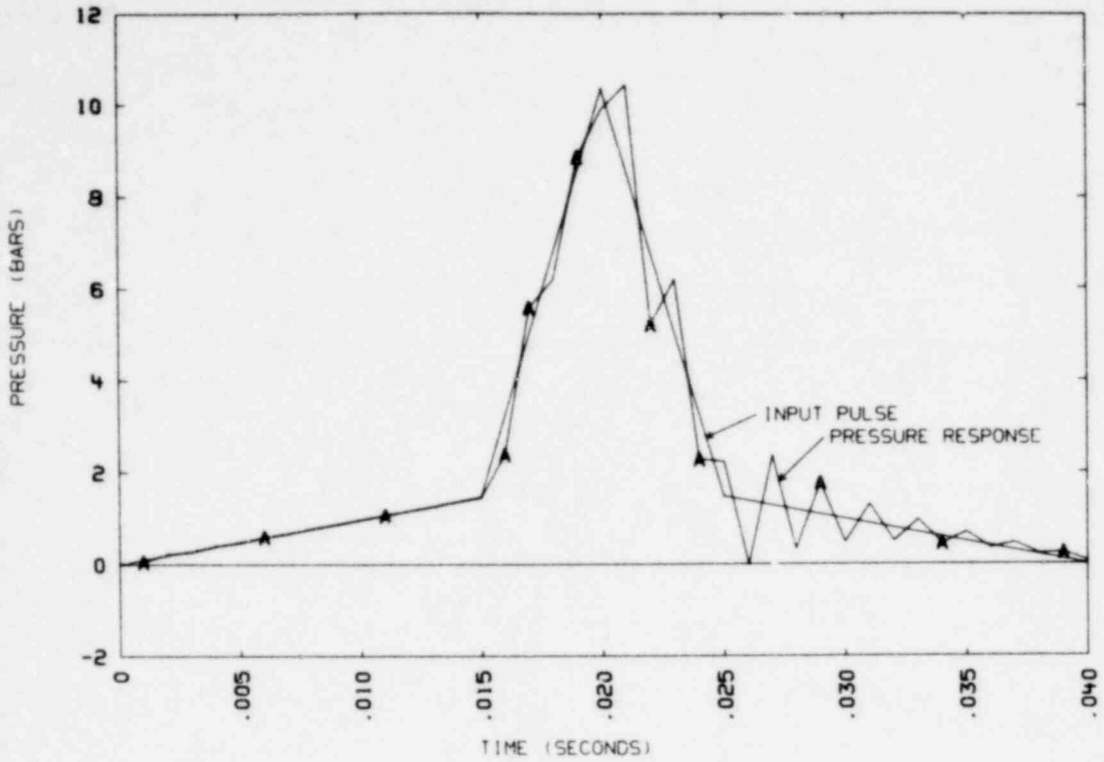

FIG. 17. Pressure response at bottom of bubble (three-dimensional slab, dt = 1.0 ms).

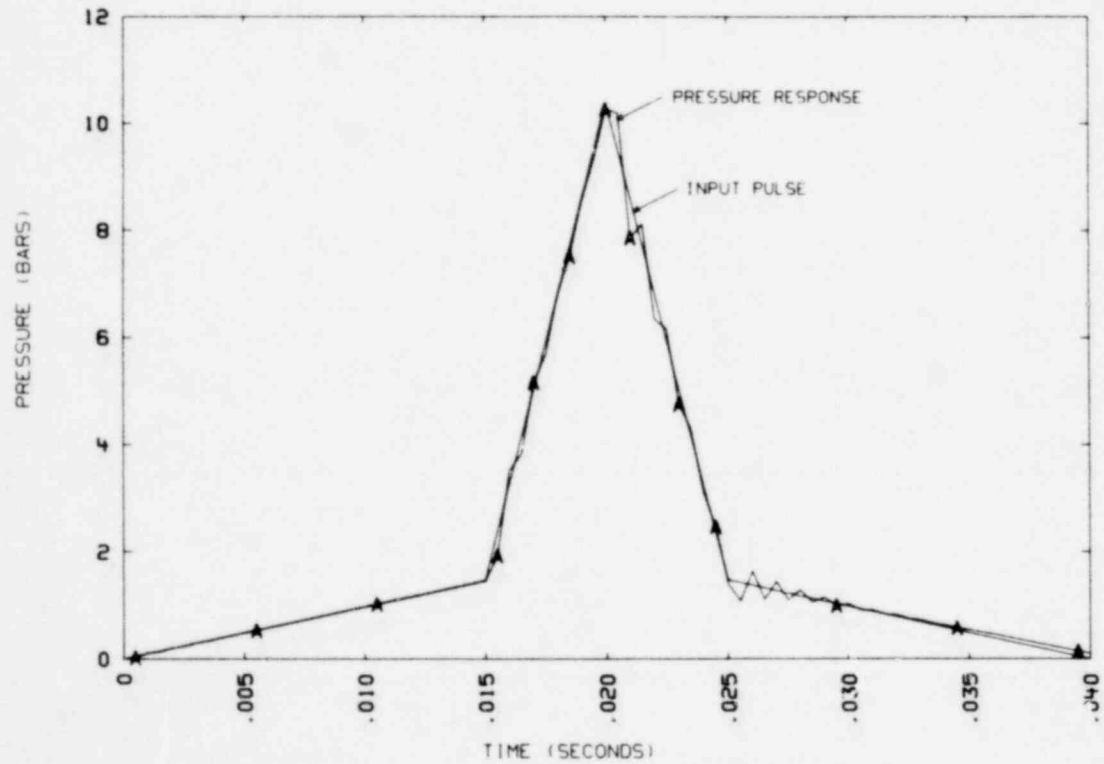

FIG. 18. Pressure response at bottom of bubble (three-dimensional slab, dt = 0.5 ms).

The effect on the pressure trace at the pool bottom, however, appears to be slight (see Fig. 19), and therefore the original 1.0 ms time step was retained for subsequent calculations.

Similar pressure and displacement comparisons were made between two- and three-dimensional plane-strain analyses for shell diameter-to-thickness ratios of 0 and 600. As indicated in Fig. 20 and in Table 1, excellent agreement was again observed between the two model types. The slight discrepancy in peak pressure at the pool bottom predicted for the rigid shell is most likely a result of the fact that the three-dimensional shell rigidity was defined by locking all of the shell nodes absolutely, while shell rigidity in the DTVIS2 model was defined by material properties (i.e., through a very large Young's modulus). The higher peak pressure predicted by the three-dimensional analysis suggests that a trace of wall flexibility is still present in the rigid DTVIS2 model.

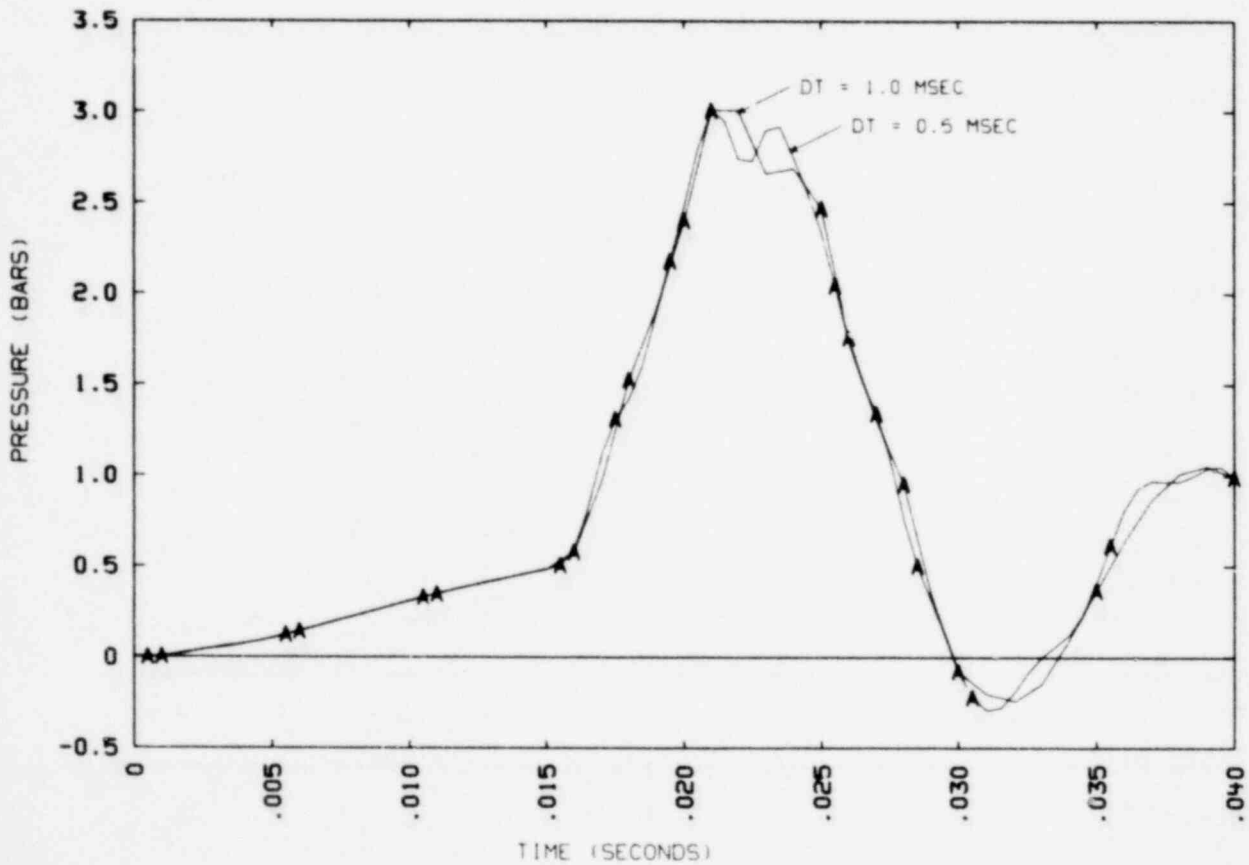

FIG. 19. Comparison of pressure response predicted at pool bottom for time steps of 0.5 ms and 1.0 ms (three-dimensional slab).

1317 244

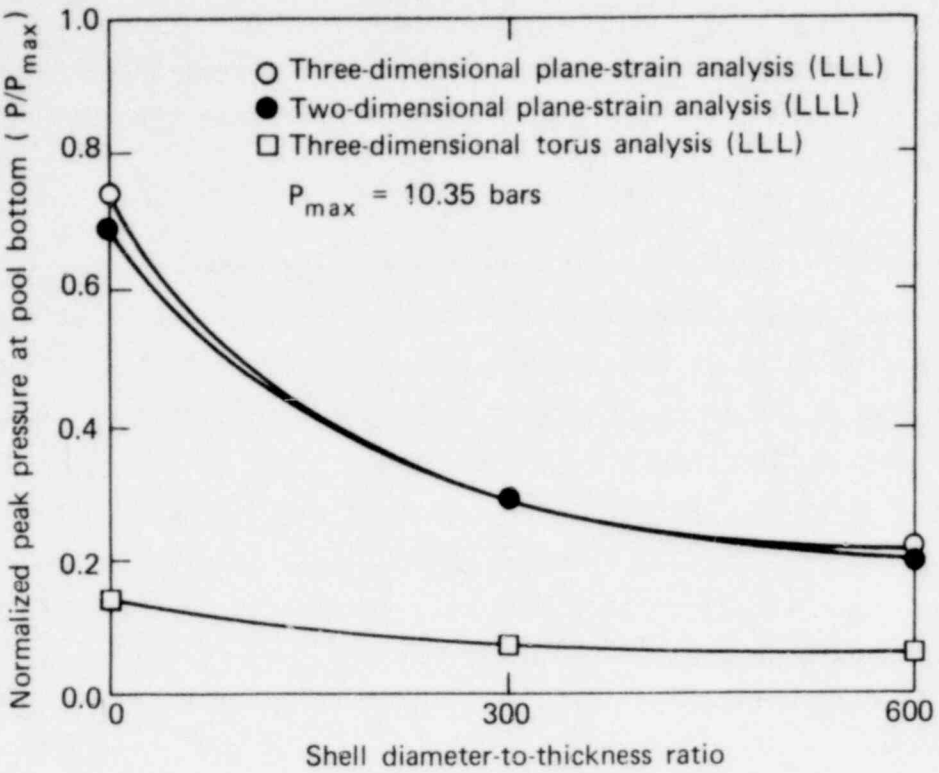

FIG. 20. Comparison of peak pressures calculated at pool bottom by two- and three-dimensional SRV analyses.

TABLE 1. Comparison of peak pressures[a] predicted at the pool bottom by two- and three-dimensional plane-strain analyses.

Shell D/t	Two-dimensional plane-strain	Three-dimensional plane-strain[b]
0	0.70 (1.0)	0.73 (1.0)
300	0.29 (0.41)	0.29 (0.40)
600	0.20 (0.28)	0.21 (0.29)

[a]Pressures are normalized to the peak source pressure (10.35 bars). Numbers in parentheses indicate pressures normalized to that calculated for the rigid shell by the type of analysis indicated.
[b]Pool bottom is in the plane of the bubble.

Because the computer time required to run the three-dimensional slab analyses was approximately one-tenth that required for the full SRV torus problems (due primarily to the very small bandwidth of the slab problem), the slab geometry proved valuable as a debugging tool for SAP4 and for the larger torus problem. Through these analyses it was determined, for example, that proper recovery of pressure in the fluid required separate calculation of the hydrodynamic and deviatoric stress components in the fluid elements. The slab analyses also provided a useful check on the method used to define the pressure on the bubble inner surface.

Three-Dimensional Torus Analytic Model

The analytic model used for the three-dimensional SRV analyses (Figs. 21 and 22) is a one-eighth section of a right circular cylindrical shell 421.7 cm in radius filled with water to a level 91.4 cm below that of the shell centerline. The ramshead SRV discharge header used in the actual system is modeled by a quarter section of a single 25.4 cm diameter bubble, cut by the two planes of symmetry in the problem and located 279 cm below the elevation of the shell centerline. The 22.5-degree angle on the ends of the actual torus bay is neglected to take advantage of symmetry in the problem. Because the radial distance from the bubble center to the end of the bay is significantly greater than that to the pool bottom, the neglect of end effects is assumed to have no effect on the pressure history directly below the bubble during the time period of interest.

The problem uses 1818 nodal points to form the finite element mesh, yielding 5138 degrees of freedom for the two cases using a flexible shell and 4646 degrees of freedom for the rigid shell case. A total of 1425 eight-node three-dimensional fluid elements is used, 75 of which are defined as "zero shear" elements to simulate the slip condition at the fluid-shell interface. The steel shell is modeled by 85 four-node quadrilateral thin-shell elements. Model definition (i.e., material properties, bubble loading, etc.) is identical to that used for the three-dimensional plane-strain model.

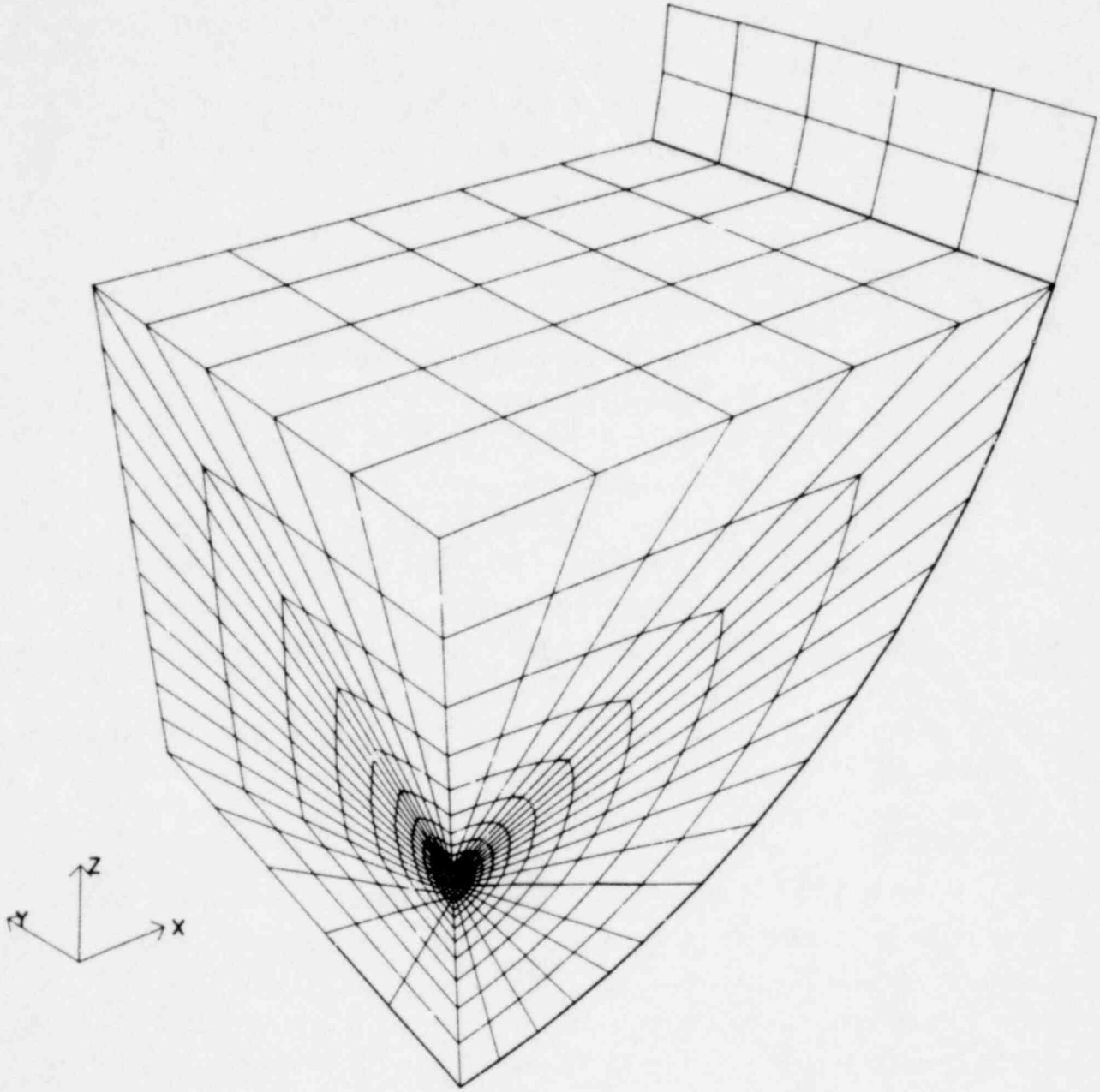

FIG. 21. Three-dimensional SRV torus finite element mesh.

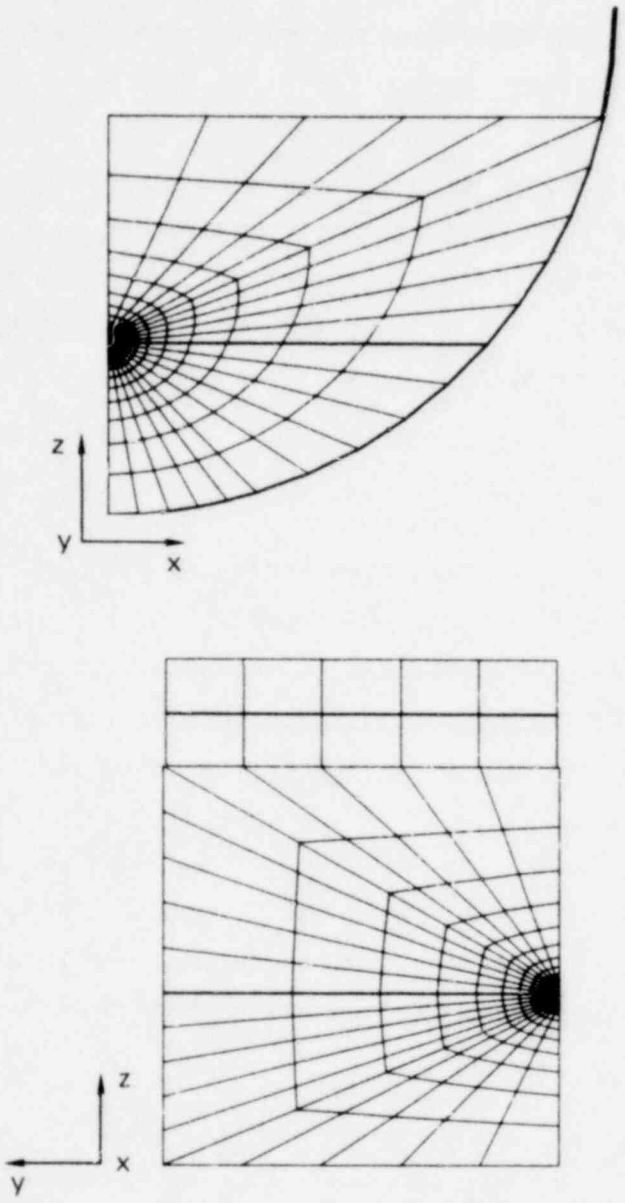

FIG. 22. Additional views of SRV torus finite element mesh.

The bubble inner surface is loaded by the same 40 ms nominal SRV pulse (Fig. 4) used for the two-dimensional DTVIS2 analyses, divided into 1.0 ms time steps. As before, the peak overpressure of the pulse is 10.35 bars. Since SAP4 will not directly accept a time-dependent pressure on a surface, it was necessary to define load components at each node on the bubble surface, corresponding to a unit pressure on the bubble and then multiply them by the pressure function used for the SRV analysis. Load components were defined by the general-purpose mesh-generating routine OASIS.[7]

Regarding boundary conditions, the shell is rigidly constrained along its upper edge for all cases. The usual symmetry conditions (i.e., constraint of out-of-plane displacements and rotations) are applied to the xz and yz planes indicated in Figs. 21 and 22. For the rigid shell case, all nodes defining the shell surface were also locked.

Three-Dimensional Torus Analyses

Results of the three-dimensional torus analyses compared qualitatively with the DTVIS2 plane-strain calculations. Figure 23 shows the pressure history in the fluid at the pool bottom,* normalized to the peak source pressure, that was calculated for shell diameter-to-thickness (D/t) ratios of 0, 300, and 600. As was predicted by the DTVIS2 analyses, the calculated peak pressure decreases with increasing D/t. In addition, the pulse shape is broadened and shifted in time as wall flexibility increases. As discussed in Ref. 3, the shift is due to early motion of the shell wall, while the broadening of the pulse is a result of momentum conservation. However, the three-dimensionality of the torus problem reduces the magnitude of the peak pressure by as much as a factor of five (see Fig. 24).

This result appears reasonable when one considers that the spherical bubble used in the three-dimensional problem is significantly less energetic than the cylindrical source implied by the DTVIS2 planar model. Furthermore, the

---

*Except where noted otherwise, the term "pool bottom," when applied to the three-dimensional torus analyses, refers to the bottom of the pool in the plane of the bubble.

1317 249

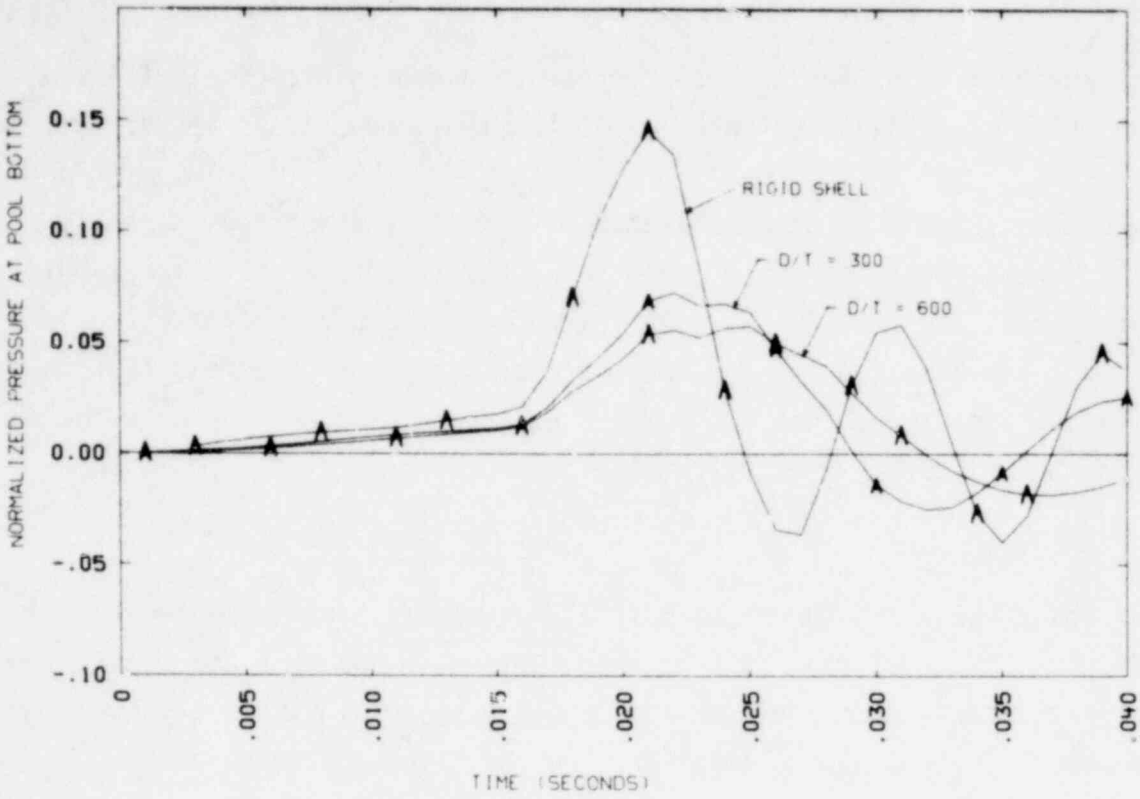

FIG. 23. Pressure response at pool bottom (three-dimensional SRV torus).

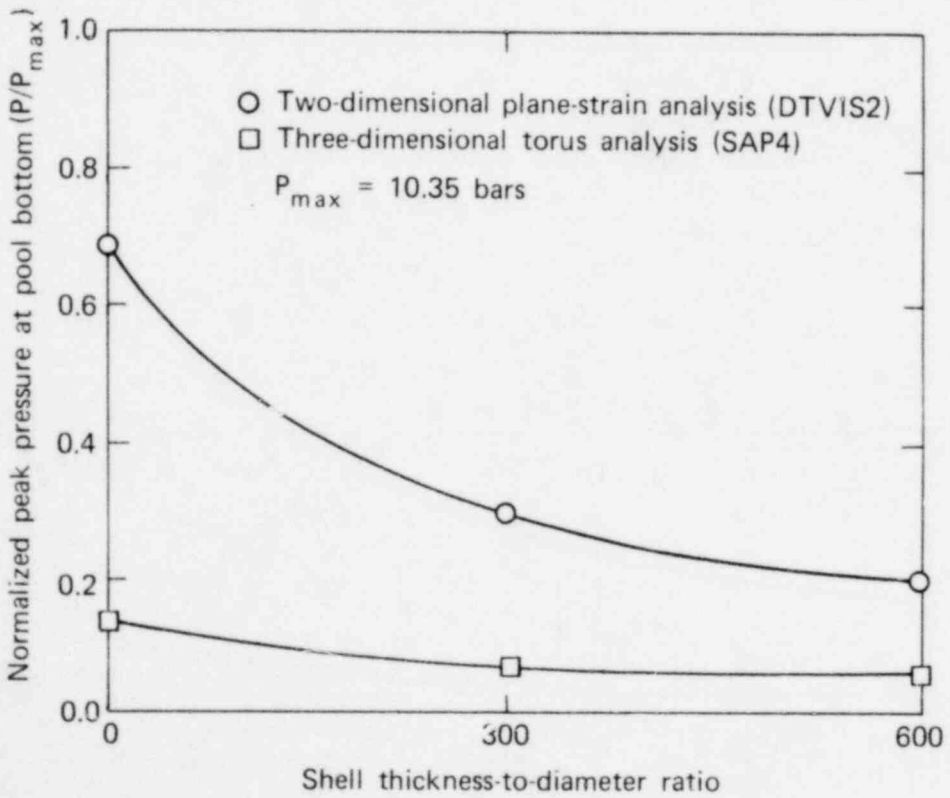

FIG. 24. Comparison of peak pressures calculated at pool bottom by two-dimensional plane-strain and three-dimensional torus SRV analyses.

three-dimensional torus has an added degree of out-of-plane (i.e., the plane of the bubble) flexibility not present in the two-dimensional representation.

Peak pressures calculated along the pool bottom at locations not directly beneath the bubble show a marked decrease as axial distance from the bubble plane increases (see Fig. 25.). Peak pressure at the pool bottom at the end of the torus bay is approximately one order of magnitude less than that in the bubble plane, indicating that the neglect of the 22.5-degree angle on the end of the bay has no apparent effect on the peak pressure calculated in the bubble plane.

A comparison of two- and three-dimensional results is also presented in Table 2. We believe it important to note that while the absolute magnitudes of the pressures calculated by the torus analyses are significantly lower than those predicted by the planar analyses, the relative magnitudes of the pressures calculated by both the two- and three-dimensional models compare well when each is normalized to the corresponding rigid wall case.

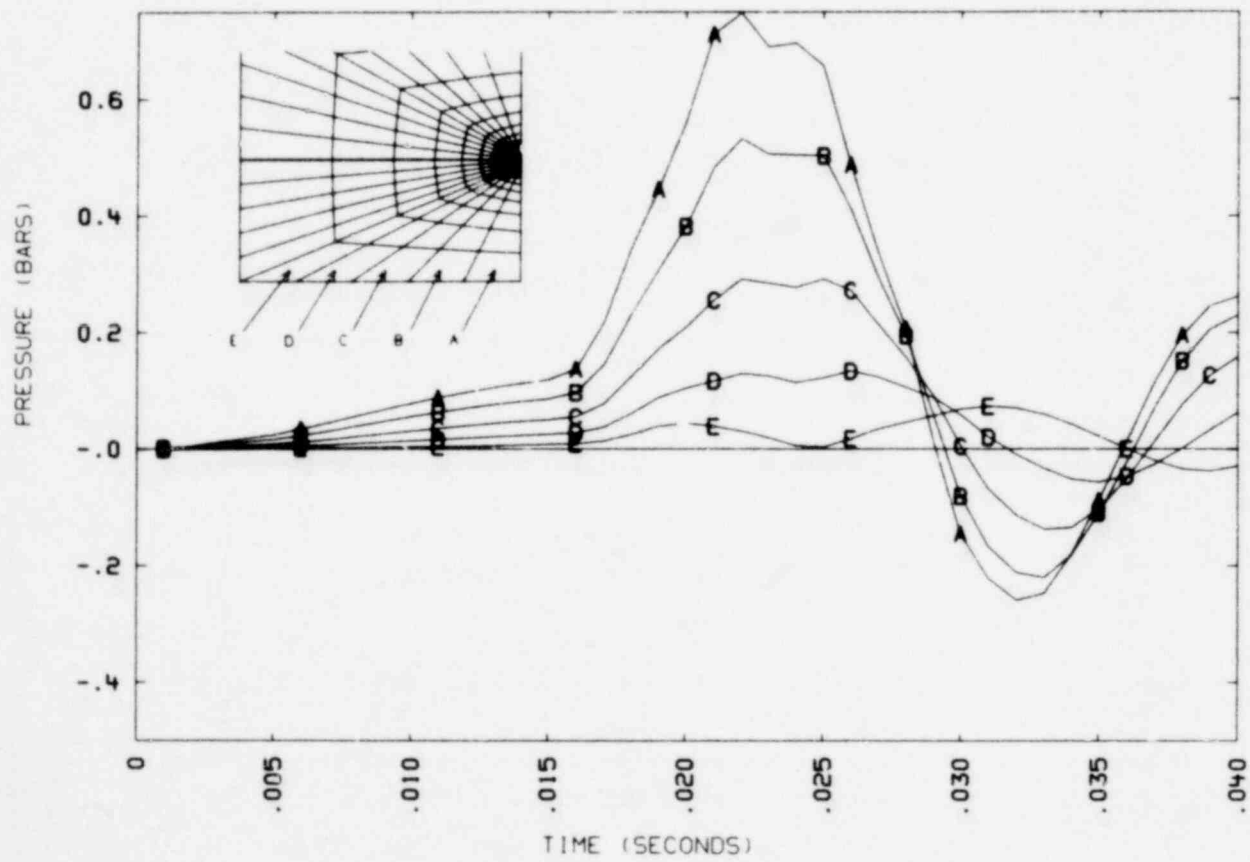

FIG. 25. Pressure histories at indicated locations along the pool bottom.

TABLE 2. Comparison of peak pressures[a] predicted at the pool bottom by two- and three-dimensional SRV analyses.

Shell D/t	Two-dimensional plane-strain	Three-dimensional[b] torus
0	0.70 (1.0)	0.145 (1.0)
300	0.29 (0.41)	0.072 (0.50)
600	0.20 (0.28)	0.057 (0.39)

[a]Pressures are normalized to the peak source pressure (10.35 bars). Numbers in parentheses indicate pressures normalized to that calculated for the rigid shell by the type of analysis indicated.

[b]Pool bottom in the plane of the bubble.

Conclusions

The results of the three-dimensional SRV analyses support the general conclusion drawn from the two-dimensional analyses; namely, that torus wall flexibility will decrease the maximum pressures seen by the shell wall. The three-dimensional results further indicate that two-dimensional hydrodynamic loads are conservative relative to three-dimensional loads for a given shell thickness, a conclusion that appears reasonable when the effectiveness of the three-dimensional pool as an energy sink, as well as the added flexibility of the three-dimensional shell, is considered.

LOCA-INDUCED HYDRO/STRUCTURE INTERACTION

A hypothetical loss-of-coolant accident (LOCA) can be divided into two stages. During the early stage--LOCA downcomer clearing--air, followed by steam, is injected into the pressure suppression pool through pairs of downcomers connected to the reactor primary containment through a ringheader and vent pipes. LOCA downcomer clearing causes a large flow rate and large pool motion. On the other hand, chugging, which occurs during the later stage of a LOCA, is caused by rapid condensation of steam bubbles formed at the downcomer exits.

Because of the large flow rate and pool motion involved, the LOCA downcomer clearing phenomenon presents an extremely complex hydro/structure interaction problem for analytical solution. The CHAMP code, earlier in development by LLL's H Division for NRC's Division of Reactor Safety Research, was originally slated for investigating this problem. Developmental difficulties with CHAMP, primarily associated with large computer time requirements and numerical instability, caused this task to be held in suspension in FY77.

In FY78, code development activities at LLL's H Division were redirected from CHAMP to a new code, PELE-IC,[8] which is based on an incompressible Eulerian formulation coupled with a thin-shell finite element code. The new code's development, however, has not progressed to the point of a well-verified production version that could be used in solving the LOCA downcomer clearing problem. Consequently, the activity in this program with regard to LOCA-induced hydro/structure interaction has been restricted to the LOCA chugging problem.

The approach to the LOCA chugging problem is similar to that employed in solving the SRV discharge problem. Air bubbles with a prescribed pressure history are assumed to form at the pair of downcomer exits. There is very little quantitative information on the shape and frequency content of chugging pulses resulting from steam bubble condensation during the later phase of a

LOCA in the Mark I BWR torus. In FY77, agreement was reached with the NRC to use a single triangular pulse with an amplitude of 20 psig (1.4 bars) and a duration of 80 ms as the nominal bubble pressure pulse for LOCA chug analyses.

The two-dimensional finite element model used in the study is presented in Fig. 26. The model is fixed at the shell waist and restrained in the horizontal direction at the vertical symmetry plane.

Linear two-dimensional LOCA chug analyses, using the nominal input pulse, were completed for torus D/t ratios of 0, 300, and 600 in FY77. Both the bottom pool pressure and the total vertical force on the torus shell were found to diminish with increasing wall flexibility. However, a lesser sensitivity was exhibited by the LOCA chug analysis as compared with the results of the SRV discharge results due to the reduced pulse amplitude and longer rise time associated with the chug pulse.

FY78's activities regarding LOCA chugging include a two-dimensional pulse variation study and a limited two-dimensional nonlinear analysis. The planned three-dimensional investigation was not completed due to time constraints, although a suitable finite element mesh was prepared.

TWO-DIMENSIONAL PULSE VARIATION STUDY

The chug pulse variation study holds the pulse shape and impulse constant while varying the pulse amplitude from -30% to +30%, as shown in Fig. 27. For +30% pulse amplitude, pressure histories at pool bottom are given in Fig. 28 and histories of the vertical forces in Fig. 29. Similarly for -30% pulse amplitude, pressure histories and vertical forces are depicted respectively in Figs. 30 and 31. Finally, the peak pool bottom pressures and the peak vertical forces, as they reduce with increasing wall flexibility, are illustrated in Figs. 32 and 33.

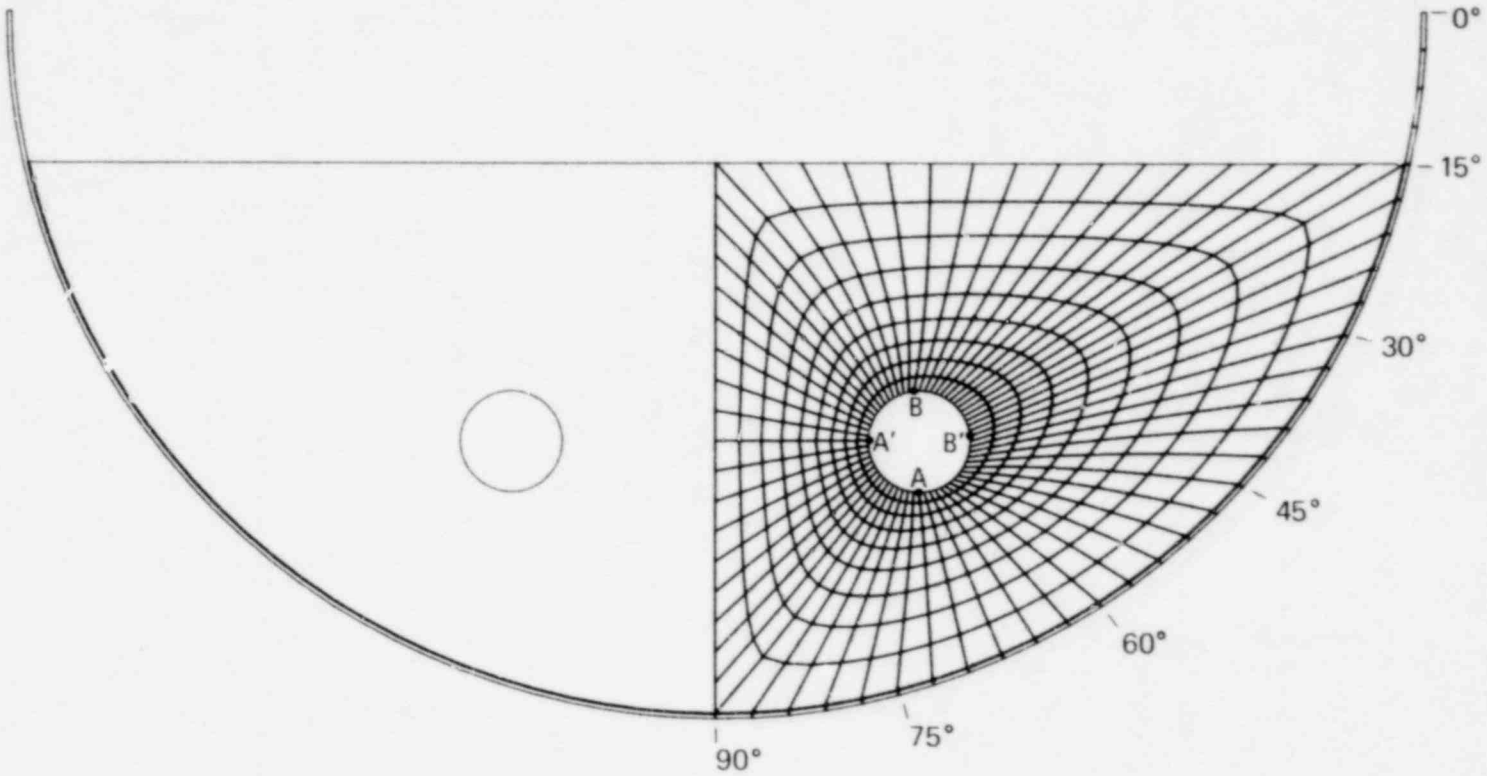

FIG. 26. Typical finite element mesh for the LOCA chug problem (D/t = 300).

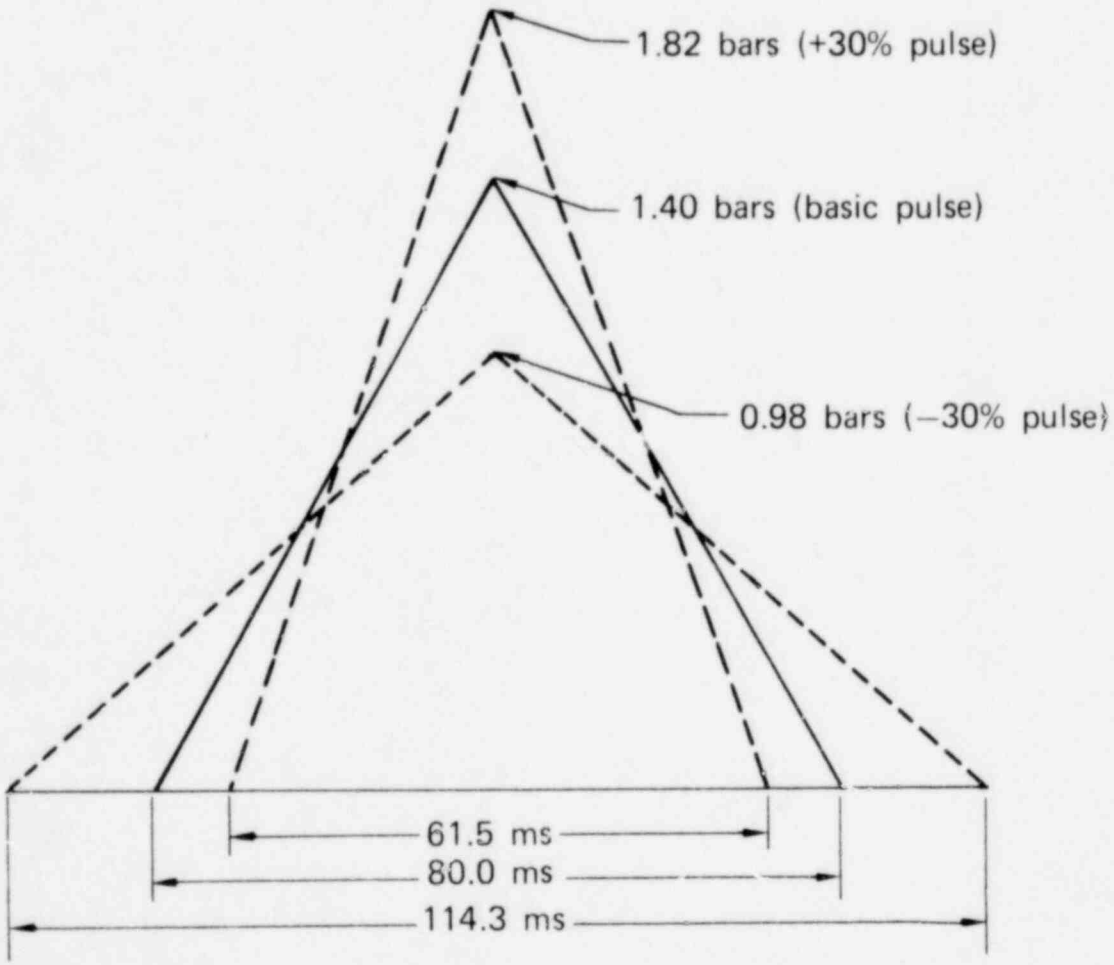

FIG. 27. Variation of LOCA chug pulses.

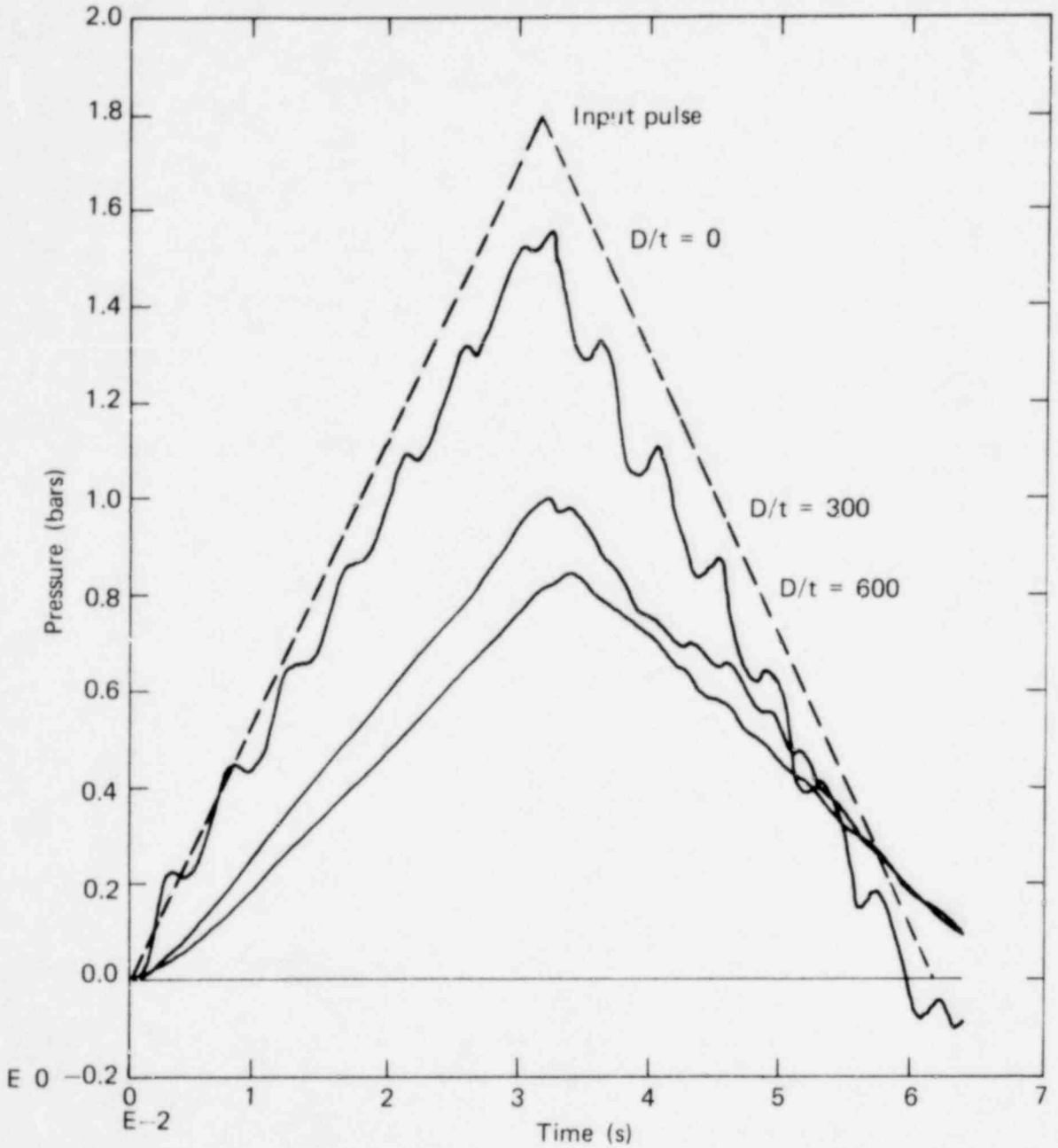

FIG. 28. Effect of torus shell thickness on pool bottom pressure history (LOCA chug +30% pulse).

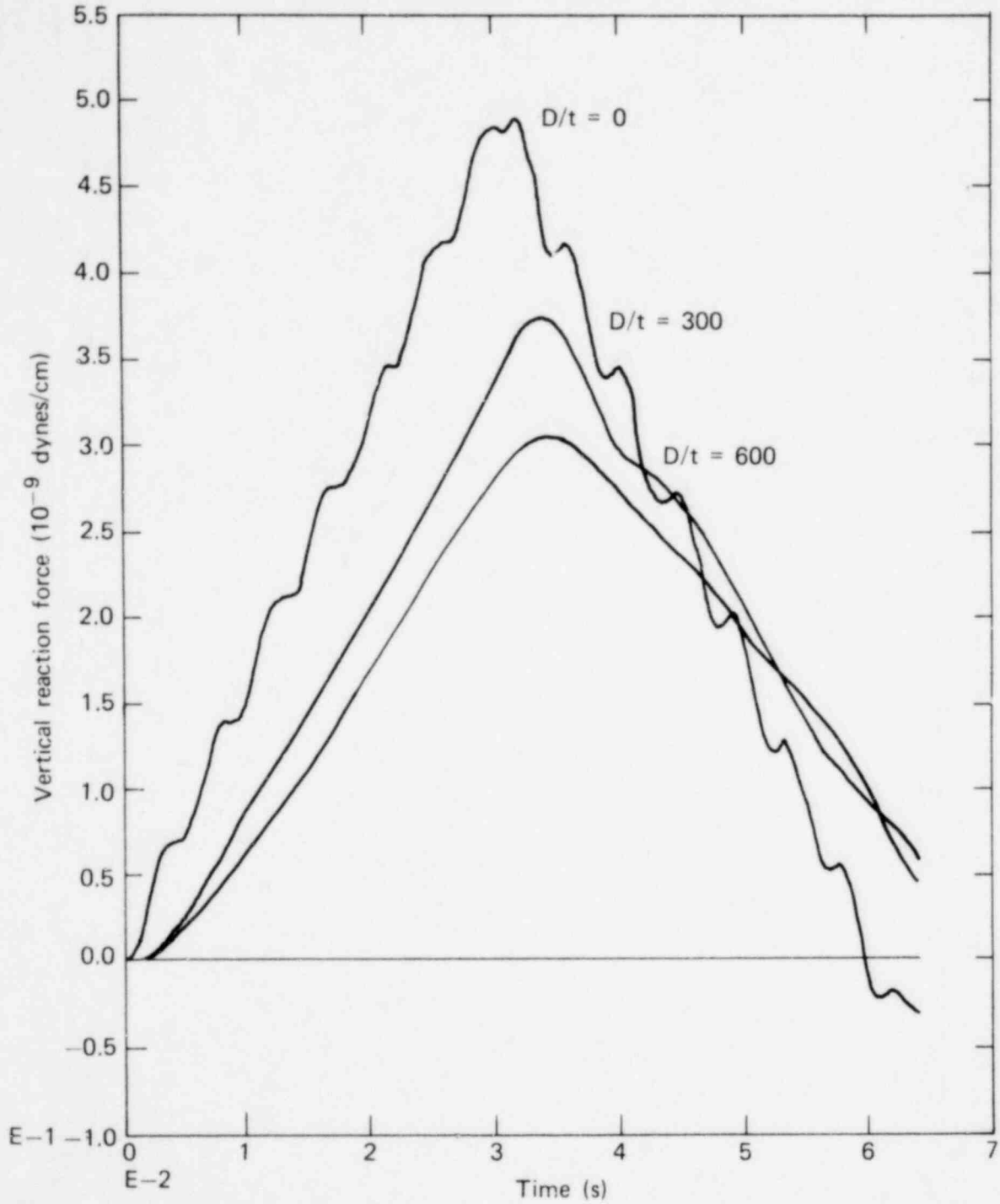

FIG. 29. Effect of torus shell thickness on total vertical force (LOCA chug +30% pulse).

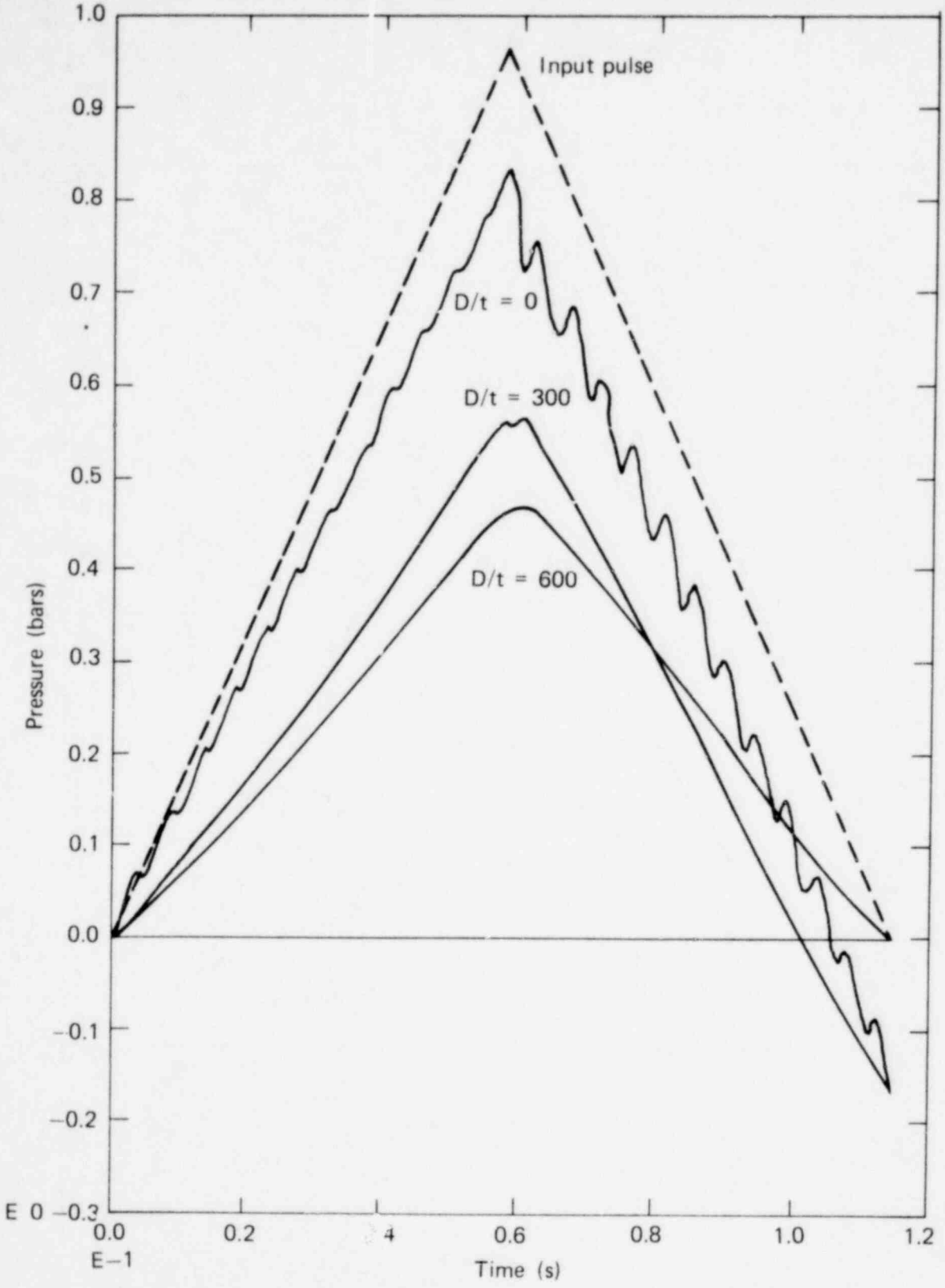

FIG. 30. Effect of torus shell thickness on pool bottom pressure history (LOCA chug -30% pulse).

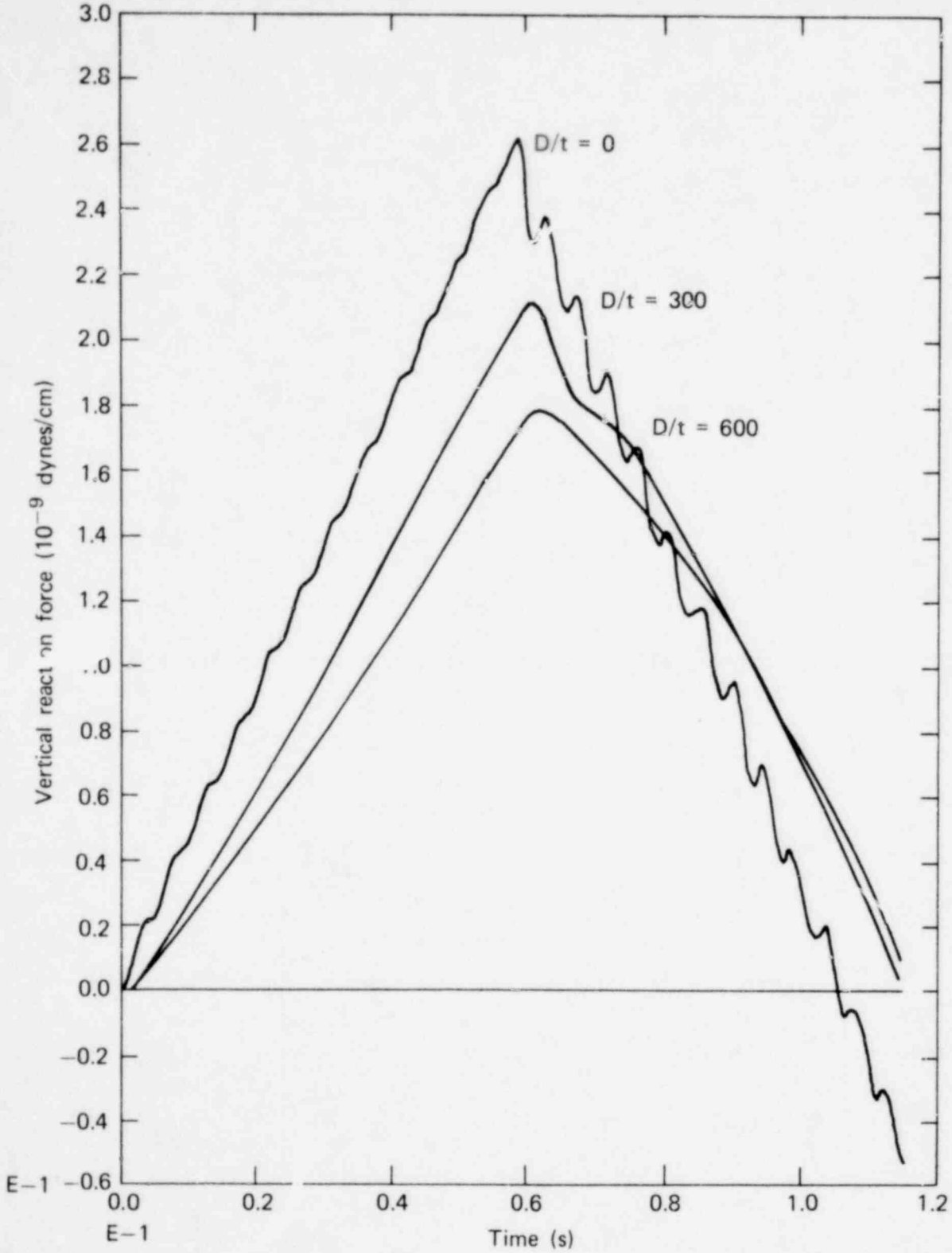

FIG. 31. Effect of torus shell thickness on total vertical force (LOCA chug -30% pulse).

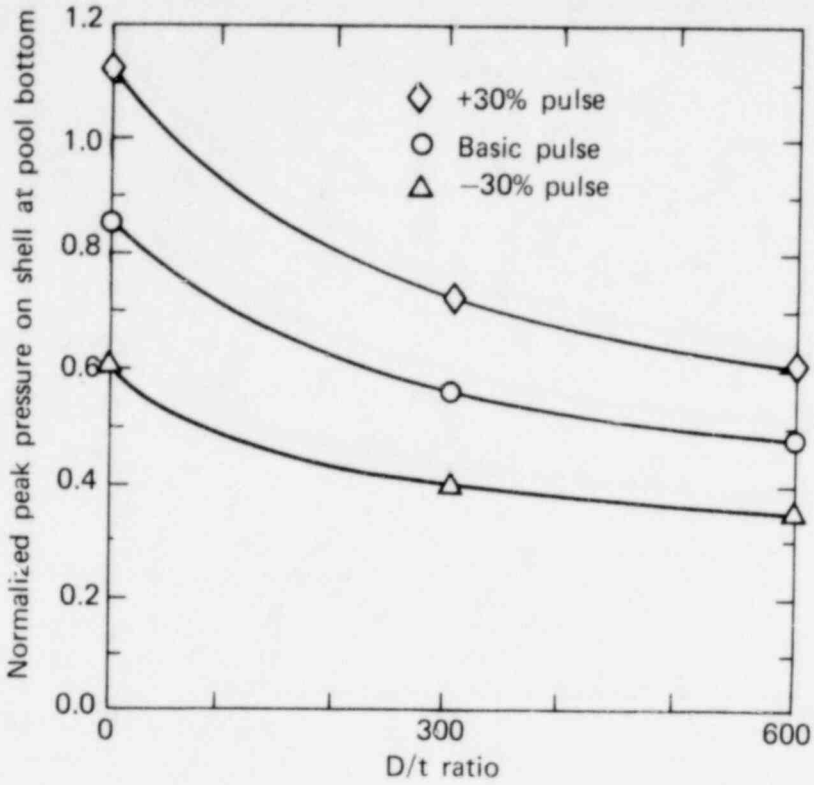

FIG. 32. Effect of torus shell thickness on normalized peak pressure at pool bottom (LOCA chug).

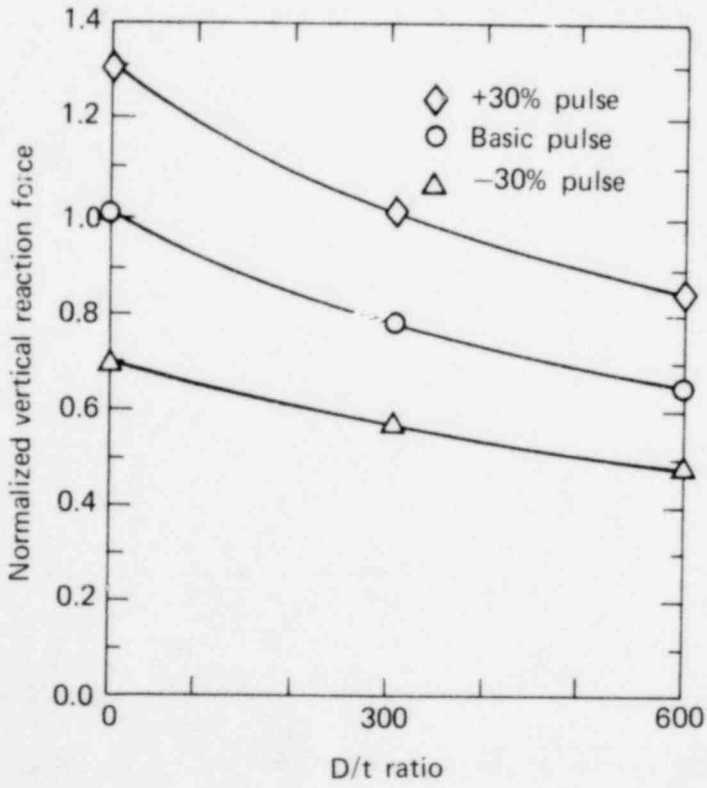

FIG. 33. Effect of torus shell thickness on normalized vertical reaction force (LOCA chug).

TWO-DIMENSIONAL NONLINEAR ANALYSIS

The pressure histories at the pool bottom are presented in Fig. 34 for both linear and nonlinear NIKE2D analyses. The basic chug pulse and D/t ratio of 300 are used in the analyses. As in the two-dimensional nonlinear analysis for the SRV discharge problem, a reduced load factor is applied to eliminate nonlinear effects in achieving a linear solution. As seen in Fig. 34, the nonlinear effect (about 15%) is of the same order as observed in the SRV discharge problem (Fig. 11).

THREE-DIMENSIONAL INVESTIGATION

A finite element mesh was prepared for a series of three-dimensional LOCA chug analyses (Fig. 35). The analytical model prepared for the chug analyses is similar to that used for the SRV analyses: a cylindrical shell 421.7 cm in radius filled with water to a level 91.44 cm below that of the shell centerline. A one-half section of a spherical bubble 30.48 cm in diameter is located with its center 121.9 cm from the vertical centerline of the shell and 259 cm below the horizontal centerline. As with the SRV analyses, the 22.5-degree angle at the end of the torus bay is neglected under the assumption of negligible end effects.

SAP4 input was prepared using this mesh for the case of a shell diameter-to-thickness (D/t) ratio of 300. The bubble inner surface was loaded by the same basic LOCA chug pulse used in the two-dimensional analyses. No analyses of the model were completed due to time considerations, program activity being deferred in favor of postprocessing activities on the three-dimensional SRV problem and in the Miscellaneous Investigations that follow.

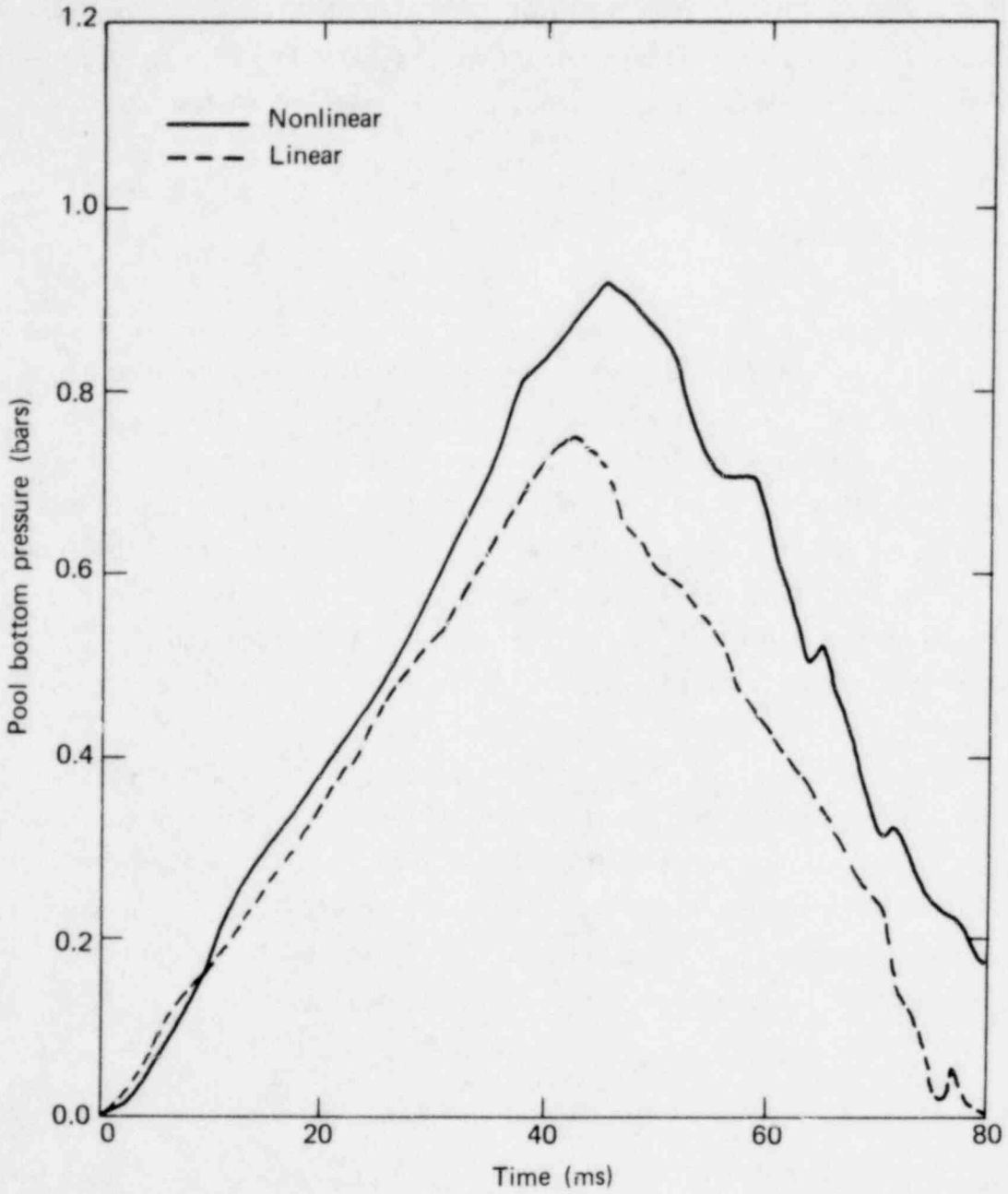

FIG. 34. Comparison of NIKE2D linear and nonlinear LOCA chug analyses (plane-strain analysis, D/t = 300).

1317 263

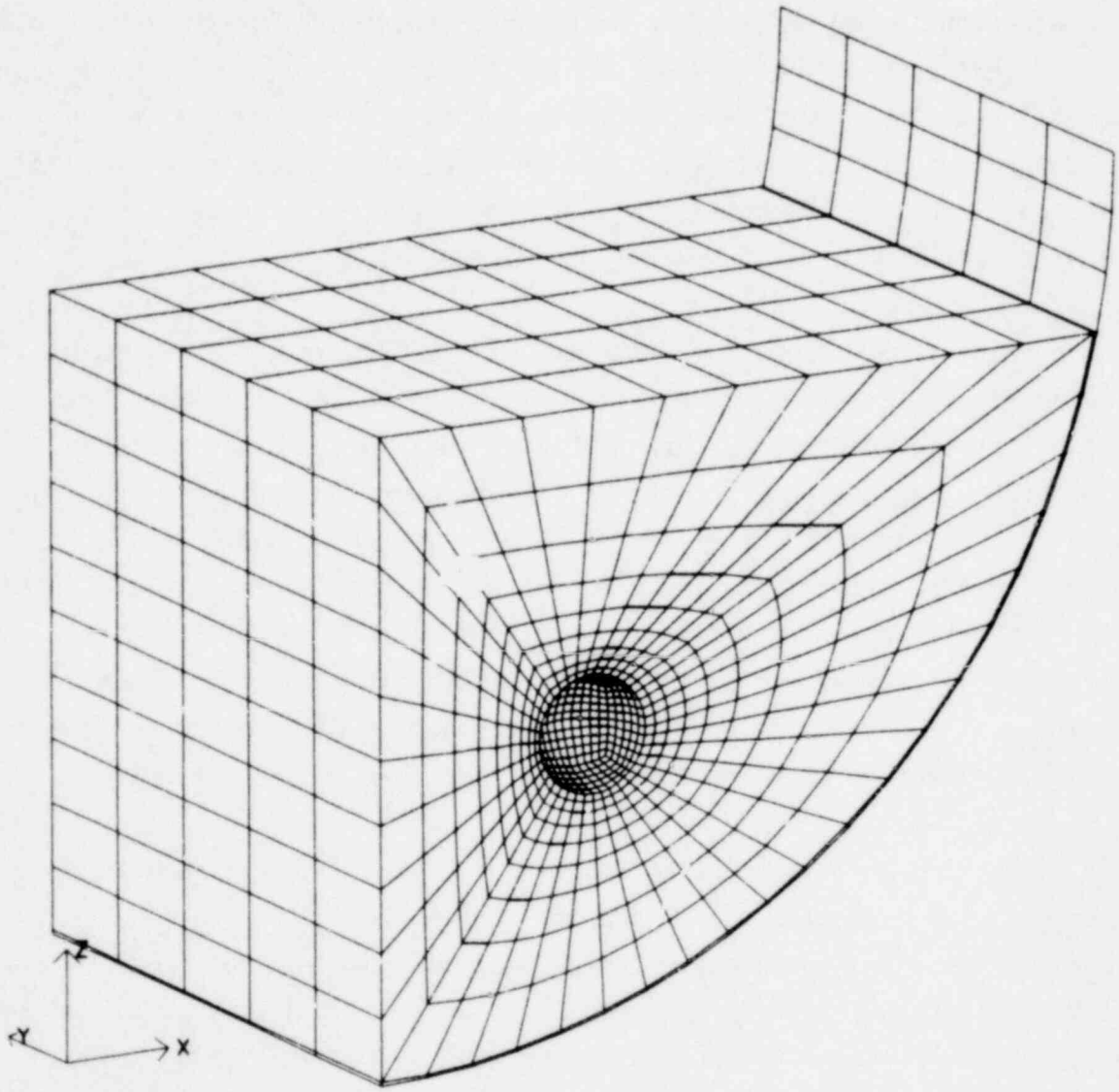

FIG. 35. Three-dimensional LOCA chug finite element mesh.

MISCELLANEOUS INVESTIGATIONS

FREQUENCY CONTENT OF SRV AND CHUG PRESSURE RESPONSES

In preparation for an NRC/LLL/Mark I Owner's Group working meeting of April 5, 1978,[9] an effort was made to identify the frequency content of both the nominal input pulses and the pressure responses at the pool bottom (SRV and LOCA chug). Due to time limitations, the response frequencies were simply estimated directly from computer plots of pressure histories at the pool bottom for each input as shown in Figs. 36 and 37.

In both cases, the pressure response for each D/t ratio considered exhibits a definite ringing at or near the end of the input pulse. The SRV ringing shows three distinct frequencies of approximately 268, 307, and 333 Hz for D/t ratios of 0, 300, and 600, respectively. The corresponding chug ringing, on the other hand, is independent of D/t at a frequency of about 350 Hz. In addition, during excitation, the chug response exhibits definite oscillations relative to the response carrier that are not clearly seen for the SRV case. The frequency of these oscillations is consistently higher during unloading of the system as compared to loading for each value of D/t, but no consistent behavior is observed when response at different D/t ratios are compared.

If it is assumed that the ringing response for each input represents some as yet unspecified characteristic frequency of the system, then a simple comparison based on harmonic oscillator behavior can be made for the two input pulses considered. The ringing frequencies previously discussed define characteristic periods, T, of 3.33 ms and 2.86 ms for the SRV and chug responses, respectively. Comparing these periods with corresponding input periods, τ, of 40 ms and 80 ms yields approximate τ/T ratios of 12 for the SRV case and 28 for the chug case. As shown in Fig. 38 (b), the response of a harmonic oscillator to a given input pulse more closely follows the input as τ/T increases. This effect is consistent with the predicted SRV and chug responses. Furthermore, if only the sharp spike of the SRV input pulse is

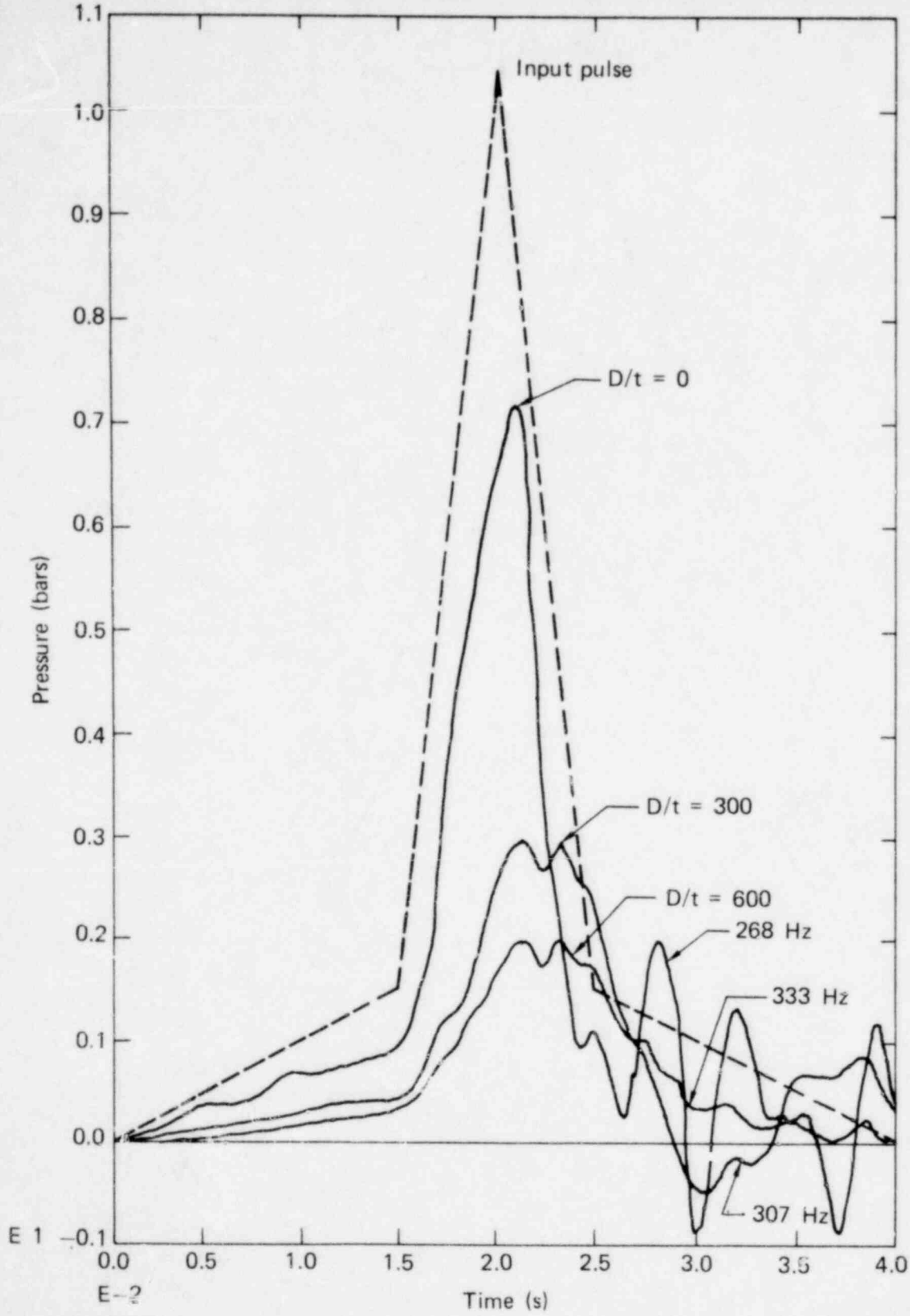

FIG. 36. Effect of torus shell thickness on the pressure history at the pool bottom (SRV discharge).

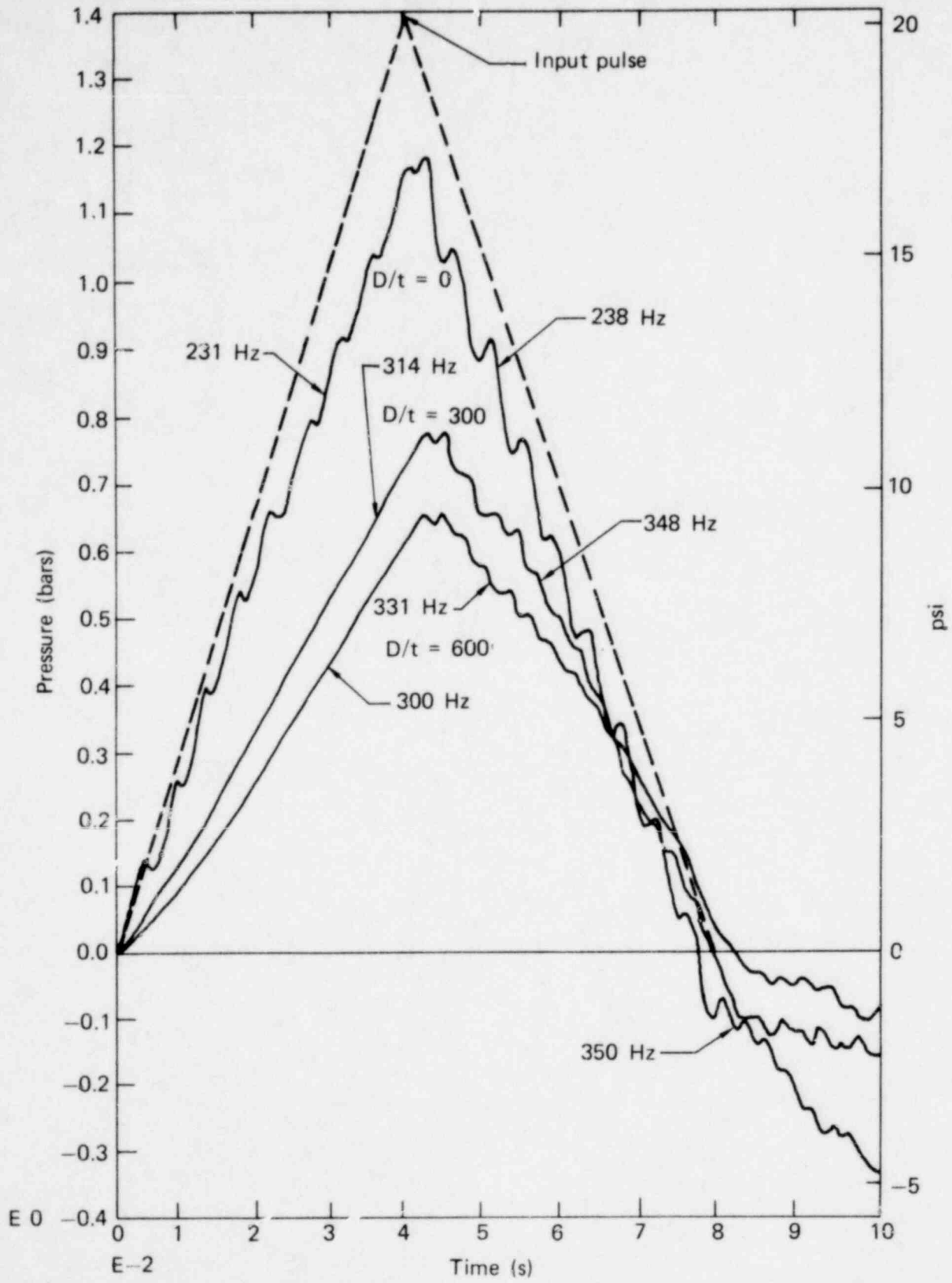

FIG. 37. Effect of torus shell thickness on pool bottom pressure history (LOCA chug).

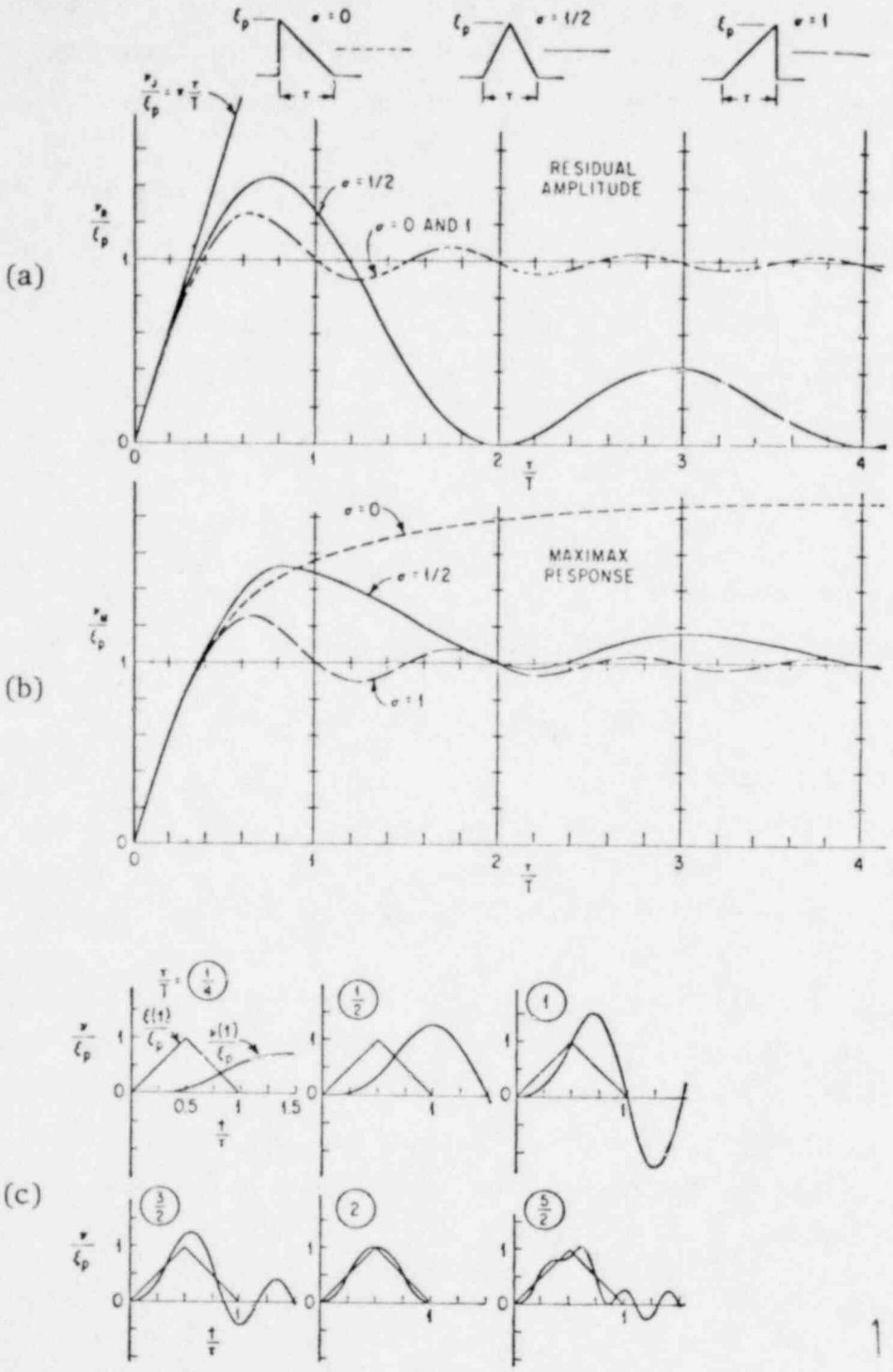

1317 269

FIG. 38. Transient response of simple harmonic oscillator to triangular forcing function. From Shock and Vibration Handbook by Harris and Crede.[10] Copyright (c) 1961. Used with permission of McGraw-Hill Book Company.

considered (τ = 10 ms, τ/T = 3), the shape of the response curves in Fig. 36 compares closely with that shown in Fig. 38 (c) for τ/T = 2.5. Although no definitive quantitative conclusions can be drawn from this simple comparison, the consistency with harmonic oscillator behavior is encouraging.

The lowest natural frequency of the global system was calculated using the relationship[10]

$$W_n = \left[\frac{Eg}{\gamma} \frac{I}{AR^4} \frac{n^2 (n^2 - 1)^2}{n^2 + 1}\right]^{1/2} , \qquad (1)$$

where

W_n = frequency for mode n-1,
E = modulus of elasticity,
γ = weight density,
g = gravitational acceleration,
R = radius of ring,
I = moment of inertia,
A = cross sectional area of ring, and
n = integer constant (for first mode behavior, n = 2).

This relationship is valid for circular rings of rectangular cross section and large radius-to-thickness ratios. For n = 2, natural frequencies of 18.9, 6.4, and 3.2 Hz were calculated for D/t ratios of 100, 300, and 600, respectively. These low values tend to indicate that the response oscillations discussed earlier result from local rather than global behavior of the analytical model.

1317 269

EVALUATION OF OTHER SRV ANALYTICAL RESULTS

This investigation provided special technical support to the NRC for the evaluation of two-dimensional and three-dimensional SRV analytical results presented by the General Electric Company at the Mark II Owner's Group Meeting on April 6, 1978, and later published as Ref. 11. LLL's analyses, conducted for comparison with GE's results from the Monticello SRV fluid/structure interaction (FSI) analysis, include the following:

A. Two linear two-dimensional plane analyses carried out to 70 ms with DTVIS2, using, respectively, thin-shell elements and 4-node quadrilateral elements to model the torus shell for a D/t ratio of 600.

B. Three linear two-dimensional axisymmetric analyses with NIKE2D for D/t ratios of 0, 300, and 600, respectively.

C. The three-dimensional SRV analyses discussed earlier in this report.

Both the plane and axisymmetric analyses use the same finite element model shown in Fig. 3. In the axisymmetric analysis, nodal coordinates are rearranged so that the model is axially symmetric with respect to the vertical symmetry axis of the torus.

Figure 39 shows the comparison of computed pool bottom pressure histories between two LLL plane analyses and GE's result. The LLL result from the shell-element model differs from GE's in two significant aspects:

- The peak pressure predicted by GE is considerably higher.
- The GE pressure history exhibits late peaks and valleys which do not appear in the corresponding LLL result.

On the other hand, the LLL 4-node quadrilateral element model predicts both a maximum peak pressure amplitude and the late peaks and valleys similar to the GE result. The close degree of comparison suggests that GE's results were likely generated by a finite element code which used overstiff 4-node quadrilateral elements instead of the more appropriate thin-shell elements to model the thin torus shell.

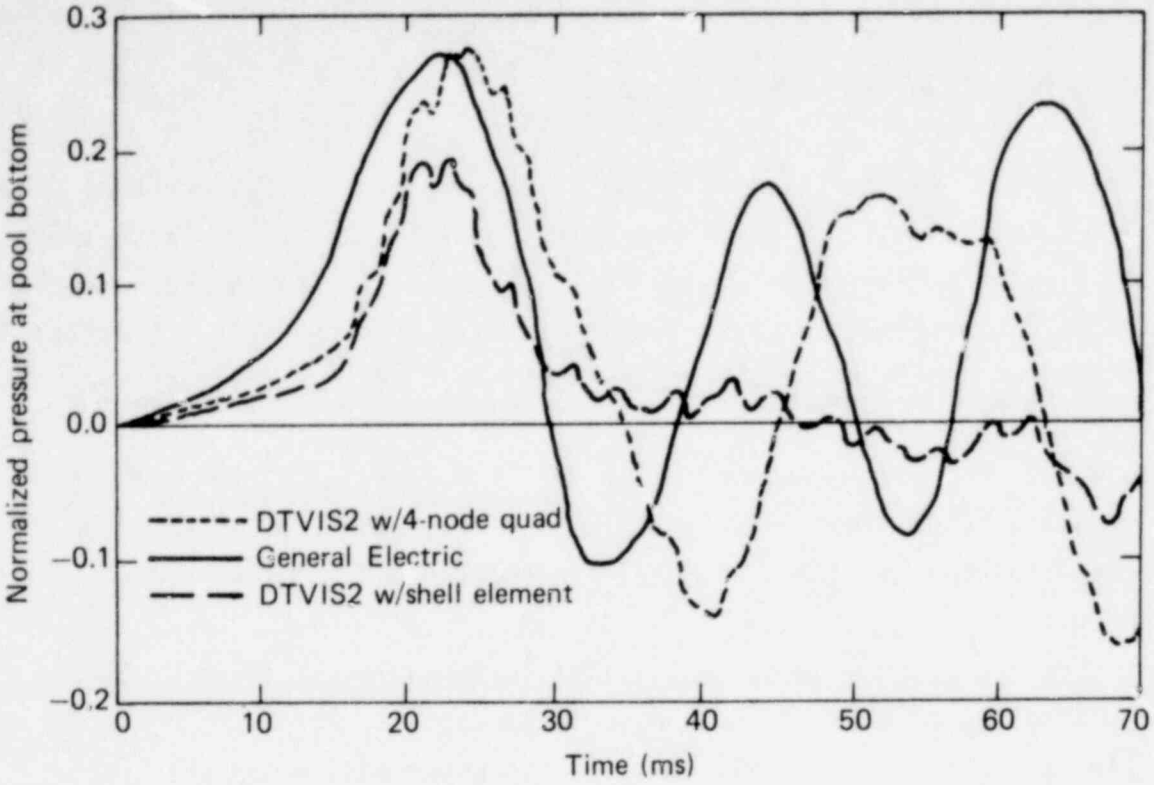

FIG. 39. Comparison of DTVIS2 SRV analysis with two-dimensional plane SRV analysis by General Electric (D/t = 600).

Figure 40 depicts pressure histories at the pool bottom predicted by LLL axisymmetric analyses for D/t ratios of 0, 300, and 600. Reduced peak pressure with increasing D/t ratio is clearly demonstrated. The LLL result for a D/t ratio of 300 is compared with the corresponding GE result in Fig. 41. Finally, normalized peak pressure variation with D/t ratio for both GE and LLL results is presented by Fig. 42.

All results except the GE axisymmetric analyses show significant peak pressure reductions with increasing D/t ratio. The exceptional behavior predicted by GE's axisymmetric analyses results from the dominant late peak in the pool bottom pressure history indicated by Fig. 41. This phenomenon could again be attributed to an inappropriate type of element being used to represent the thin torus shell.

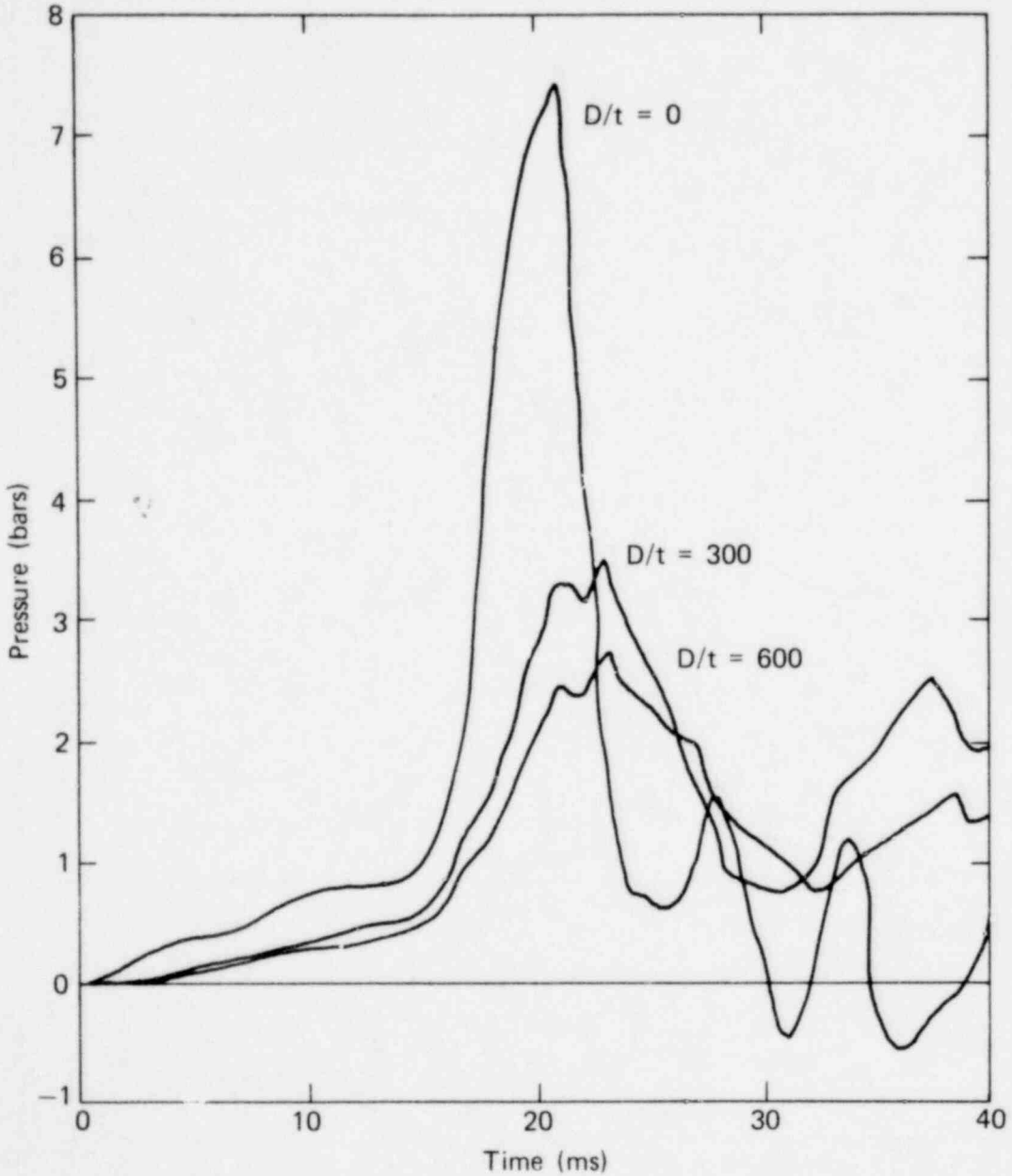

FIG. 40. Pressure histories at pool bottom (SRV basic pulse, axisymmetric analysis).

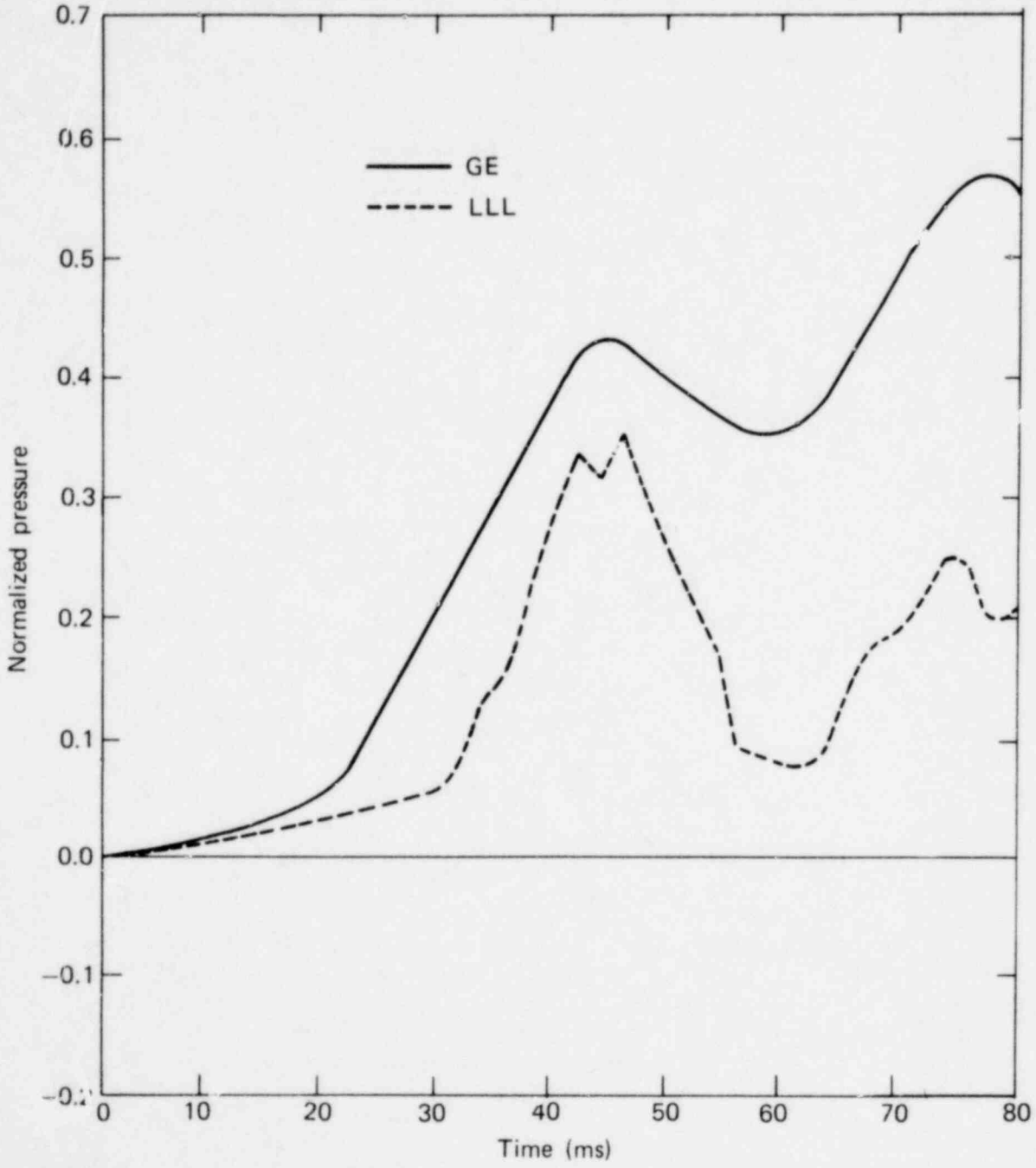

FIG. 41. Pressure history at pool bottom (axisymmetric analysis, D/t = 300).

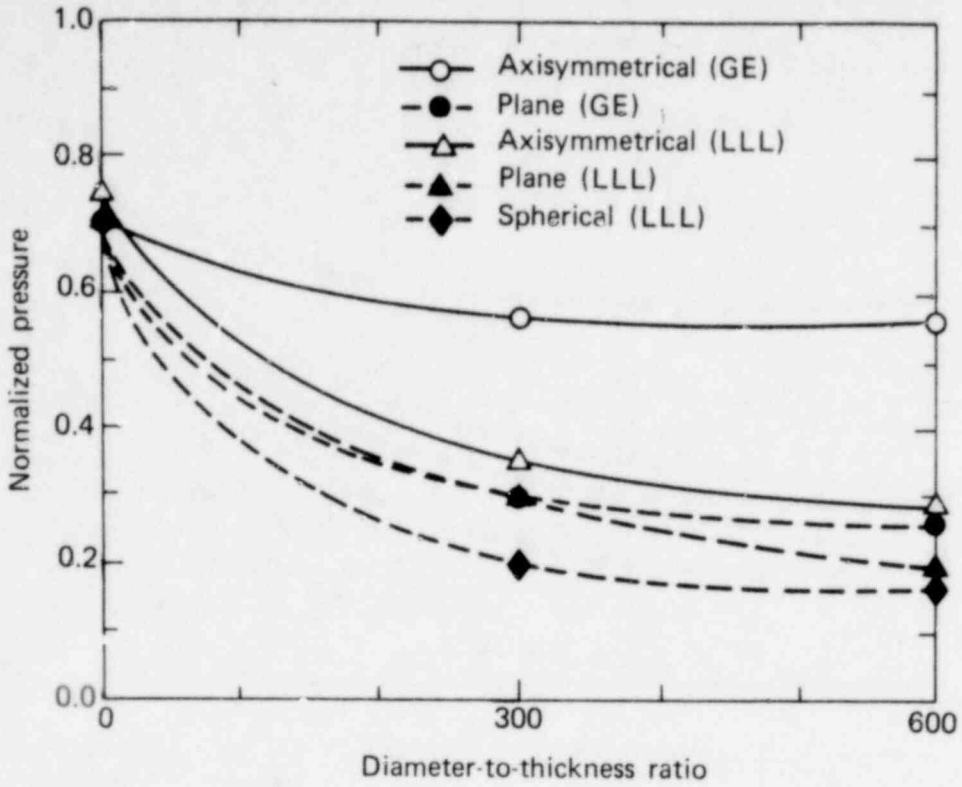

FIG. 42. Effect of wall flexibility on pool bottom pressure.

Finally, GE's three-dimensional SRV analytical results are also compared with LLL results. As shown in Fig. 43, GE's results indicate that the peak pressure at the pool bottom increases with wall flexibility, opposite the effect of wall flexibility predicted by the LLL three-dimensional results presented earlier in this report. Furthermore, the pressure magnitudes predicted by the GE three-dimensional analyses are of the same order as those predicted by the LLL two-dimensional analyses.

The technical information presented by General Electric at the April 6, 1978, meeting forms the body of a formal report[11] later released to NRC and reviewed by LLL. Overall, the report repeats the two-dimensional results that were presented (with the exception of some axisymmetric results). The three-dimensional results presented in the report (see Fig. 43) are different from those originally presented by GE and indicate that the pressure response at the pool bottom is insensitive to variations in the shell wall D/t ratio. This result is attributed to changes made in the three-dimensional finite

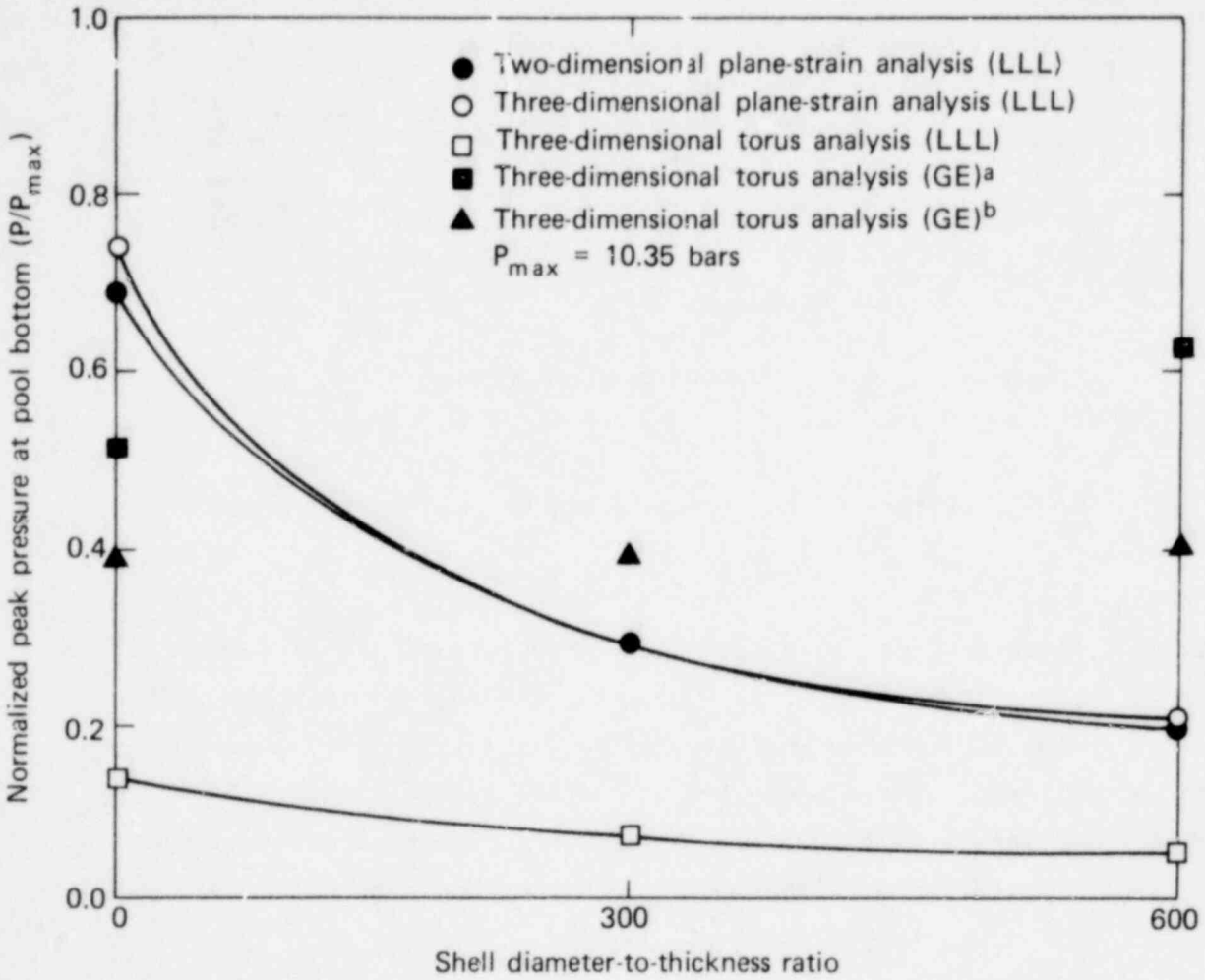

[a]Mark II Owner's Group Meeting, April 6, 1978.

[b]H. T. Tang, Fluid-Structural Interaction Analysis..., General Electric Co., NEDO-23834 (June1978).

FIG. 43. Comparison of peak pressures calculated at pool bottom by two- and three-dimensional SRV analyses.

element mesh; however, the mesh presented in the report and the one presented at the April 6, 1978, meeting appear identical. For this reason, it is difficult to appreciate the source of problem redefinition that led to the new results. Furthermore, a continued lack of detailed information about the three-dimensional SRV model used makes a detailed comparison with the corresponding LLL model essentially impossible.

FLAT PLATE USAGE FOR INVESTIGATING H/SI EFFECTS IN SHELLS

A series of dynamic two-dimensional finite element analyses has been completed investigating the applicability of using a flexible flat plate segment in an otherwise rigid shell to determine hydro/structure interaction effects on wall pressure response.

The model chosen for these analyses (Fig. 44) closely resembles that used for earlier DTVIS2 linear SRV analyses of the flexible shell (Fig. 3), except that a flexible flat plate is mounted on the inner shell wall. Using the Acurex[12] experiment as a guide only, the plate was mounted with its center 30 degrees off the shell centerline, subtending an arc of 40 degrees. The plate was pinned at its lower end (i.e., the end nearest the shell centerline) and was roller mounted at the opposite end. Plate thicknesses corresponding to shell diameter-to-plate-thickness ratios of 0, 300, and 600 were used. When compared to similar shell diameter-to-shell-thickness ratios on the basis of natural frequency, these values translate to equivalent ratios of 0, 246, and 492, respectively. Input loading on the model was by the same nominal SRV pulse (p_{max} = 10.35 bars) used in the earlier flexible shell analyses.

The first analysis was a comparison of rigid models with and without the internal plate. As shown in Fig. 45, the pressure response calculated for the pool bottom is essentially unperturbed by the presence of the plate. However, when the pressure history at the plate center is compared to that at the pool bottom (see Fig. 46), it is observed that while the character of the pressure response at each location is quite similar, the magnitude of the peak pressure at the plate center is significantly lower than that at the pool bottom. This same effect is observed when flexible plates inside the rigid shell are considered (see Fig. 47). Again, the overall character of the pressure

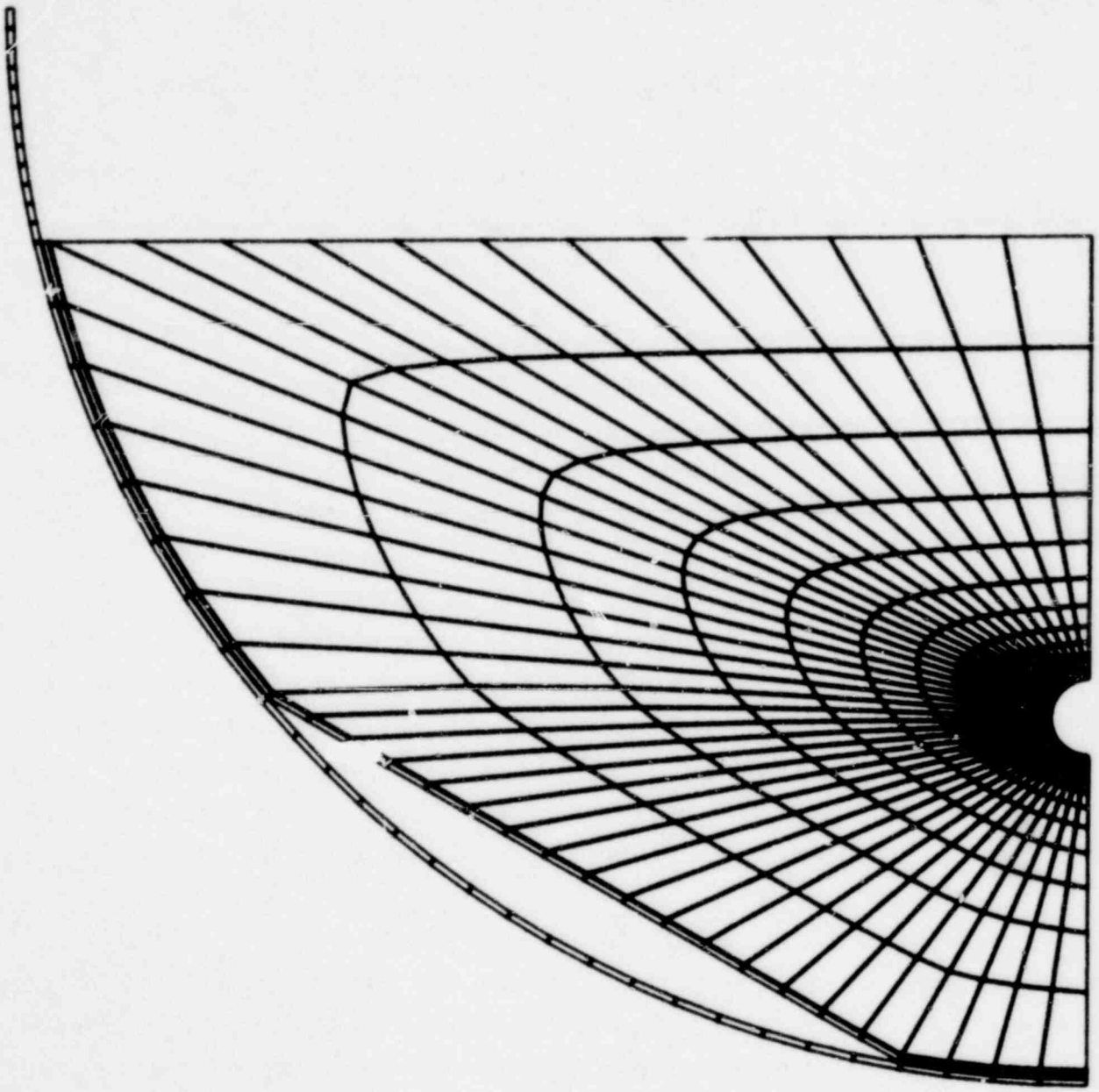

FIG. 44. Finite element mesh for SRV rigid shell with internal flat plate.

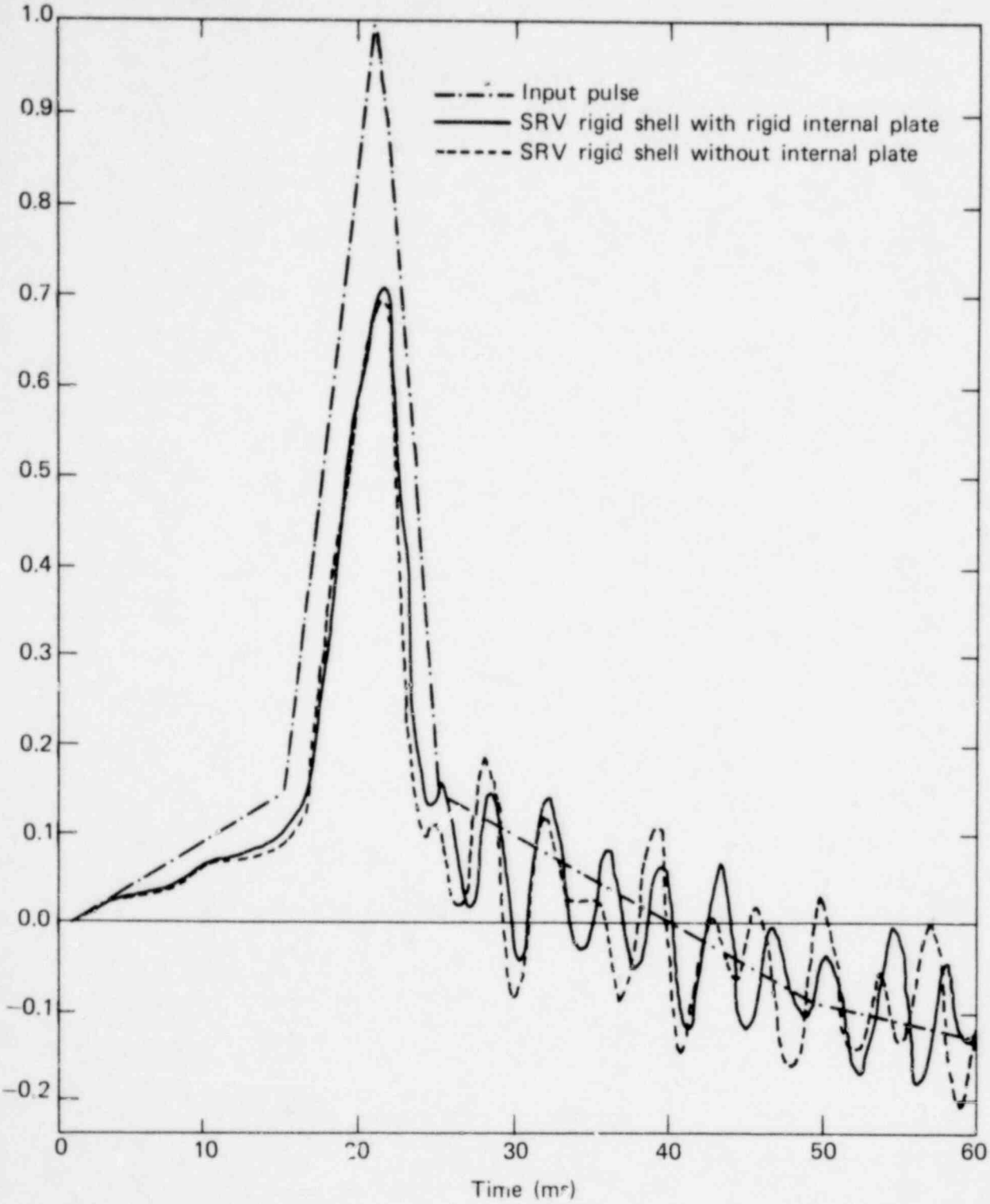

FIG. 45. Comparison of pressure response at pool bottom for rigid shell with and without internal plate.

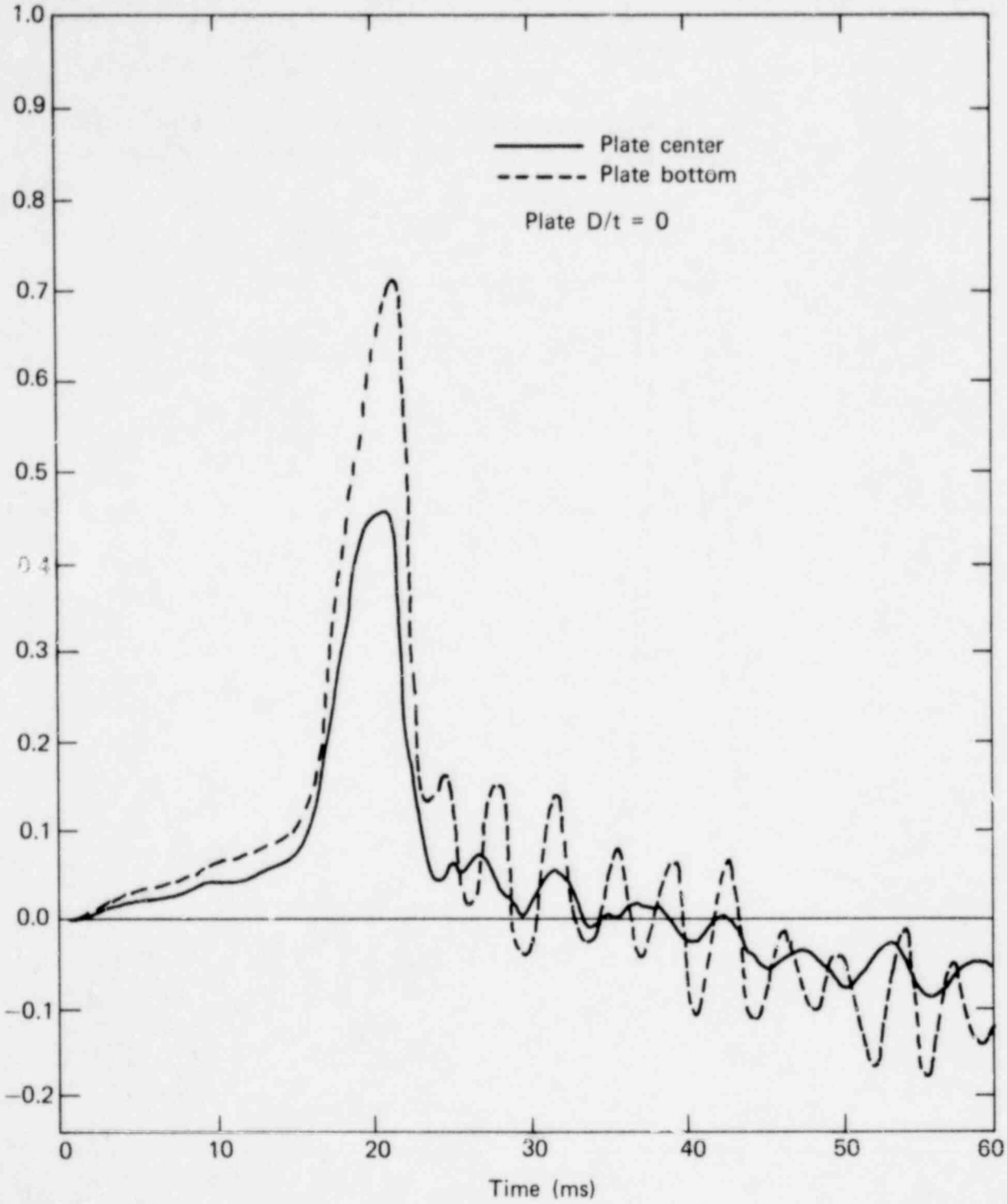

FIG. 46. Comparison of pressure response at pool bottom and plate center for SRV rigid shell with rigid internal plate.

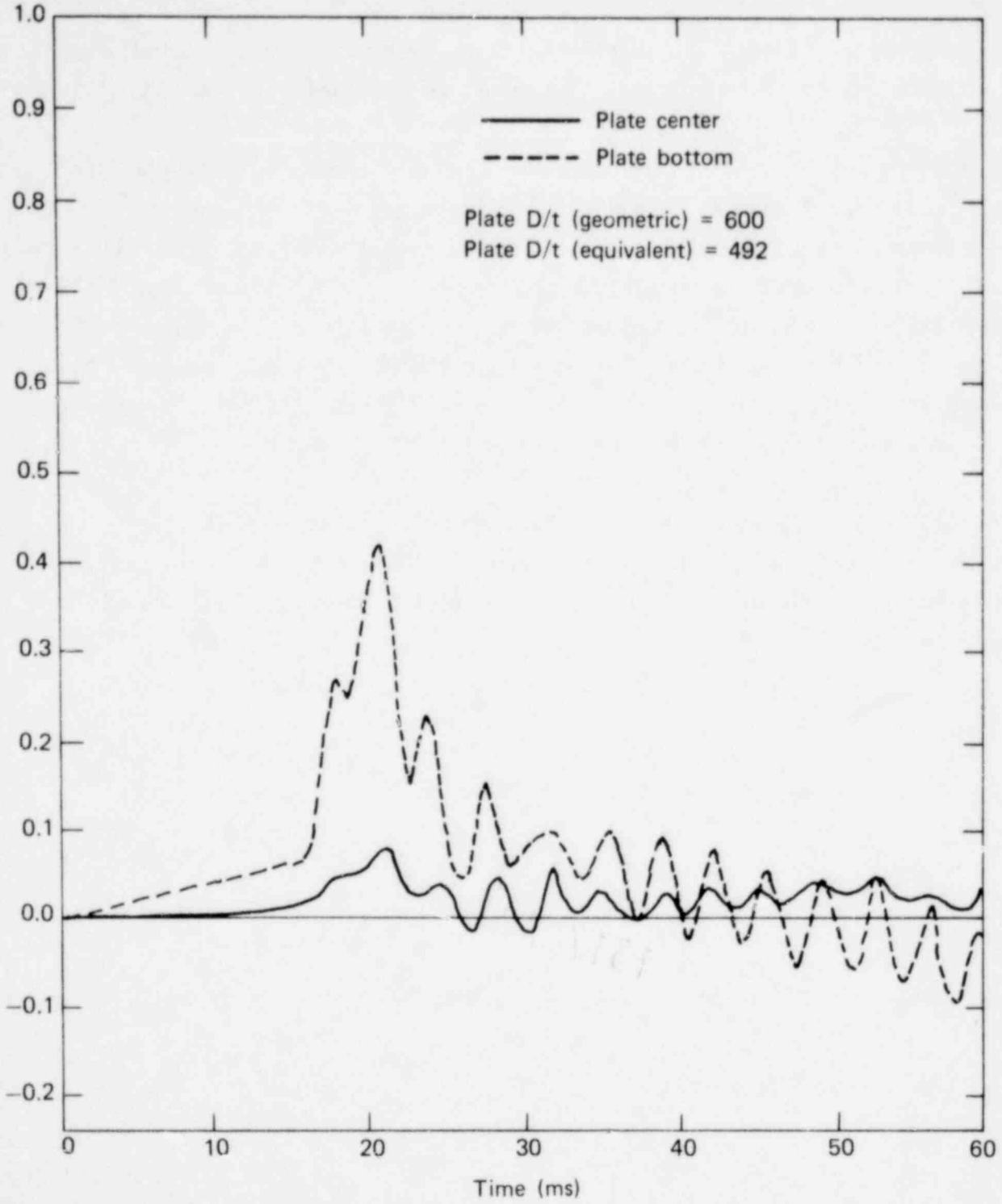

FIG. 47. Comparison of pressure response at pool bottom and plate center for SRV rigid shell with flexible internal plate.

response is similar, but the magnitudes vary significantly. A summary of peak pressure vs equivalent shell thickness-to-diameter ratio is presented in Fig. 48. It is of interest to note that the peak pressure predicted along the flat plate was found to be highly dependent on location.

A companion set of analyses was performed for a geometrically similar problem under a different loading condition. In these analyses, the bubble was positioned along the shell centerline at the elevation of the downcomer ends, then was loaded by the nominal LOCA chug pulse (p_{max} = 1.38 bars) used for the DTVIS2 flexible shell chug analyses. A comparison of the pressure response predicted at the plate center with the pressure at the pool bottom showed the same basic behavior as that observed in the SRV case, despite the less impulsive nature of the chug input pulse.

Overall, these results indicate that while the qualitative flat plate response compares well with that observed earlier for the flexible shell, the absolute pressures predicted along the flat plate vary significantly and nonconservatively.

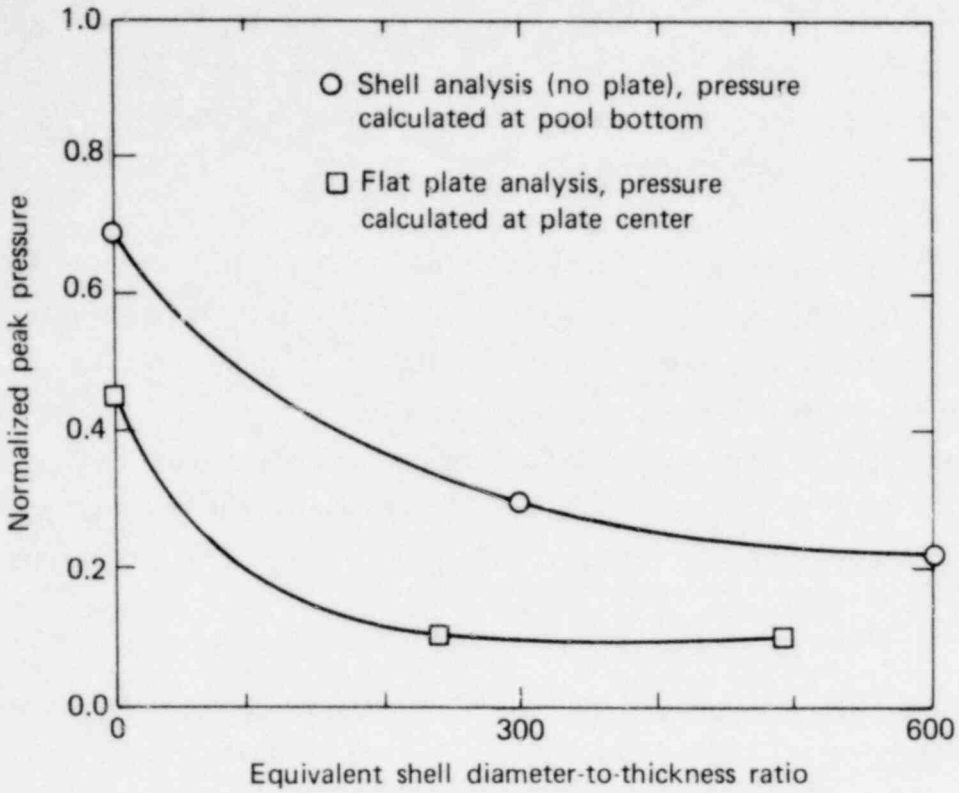

FIG. 48. Comparison of predicted fluid/structure interaction effects on peak wall pressure for flexible shell and flexible plate analyses.

CONCLUSIONS AND RECOMMENDATIONS

The general conclusions reached at the end of our FY77 project activities were that, for single pulse sources, torus wall flexibility decreases both the maximum pressure seen by the wall and the total vertical loads resulting from the hydrodynamically induced pressure. This conclusion has been further supported by the results from our FY78 activities, which include the two-dimensional pulse variation studies and limited nonlinear effect investigations for both the SRV and LOCA chug problems and the comprehensive three-dimensional SRV analyses.

Numerous load cases were considered in the two-dimensional pulse variation studies for different combinations of pulse amplitudes, pulse rise times, and torus diameter-to-thickness ratios. Although reduction of hydrodynamic loads with increasing wall flexibility was observed consistently for each of the cases, the effect of the torus wall flexibility was found to be more pronounced for a higher pulse amplitude associated with shorter rise time. The two-dimensional nonlinear investigations indicated that including nonlinear effects due to large fluid deformation does not cause serious deviation from the linear analytical results.

Results of three-dimensional analyses compared qualitatively with two-dimensional results. The calculated peak pressure decreases monotonically with increasing diameter-to-thickness ratio. In addition, the pulse shape is broadened and shifted in time as wall flexibility increases. The three-dimensionality of the torus configuration considerably reduces the magnitude of the peak pressure at all D/t ratios. This result appears reasonable when it is considered that the spherical bubble used in three-dimensional analyses is significantly less energetic than the cylindrical source implied by the two-dimensional idealization. It is important to note, however, that the relative pressure reduction offered by the flexible boundary over the rigid case is quite similar to that observed in the two-dimensional analyses.

We conclude finally that although the simple and fast two-dimensional linear analysis is a good approach for generating qualitative results, the more complex and time-consuming three-dimensional approach is necessary to produce more reasonable quantitative solutions of hydro/structure interaction phenomena associated with Mark I BWR containment.

We emphasize that the analytical work presented in this report has not received any experimental verification. To obtain a better understanding of hydro/structure interaction phenomena in the Mark I BWR pressure suppression system, future work with emphasis on verifying analytical results through empirical experimentation should receive strong attention. In addition, a development effort aimed at completing a well-verified computer code for treating the driving function produced during the LOCA air transient is required.

REFERENCES

1. E. K. Collins and W. Lai, Final Air Test Results for the 1/5-Scale Mark I Boiling Water Reactor Pressure Suppression Experiment, Lawrence Livermore Laboratory, Livermore, Calif., UCRL-52371 (October 31, 1977).
2. J. H. Pitts and E. W. McCauley, Vertical Forces Induced in a 1/5-Scale Mark I BWR Toroidal Wetwell under LOCA Conditions, Paper No. B4/6, presented at the 4th International Conference on Structural Mechanics in Reactor Technology, San Francisco, Calif. (August 15-19, 1977).
3. R. W. Martin and E. W. McCauley, The Effects of Torus Wall Flexibility on Forces in the Mark I BWR Pressure Suppression System--Part I, Lawrence Livermore Laboratory, Livermore, Calif., UCRL-52506 (June 1978).
4. J. L. McCready, et al., Steam Vent Clearing Phenomena and Structural Response of the BWR Torus (Mark I Containment), General Electric Company, Report NEDO-10859 (April 1973).
5. G. L. Goudreau, DTVIS2 User's Manual, Lawrence Livermore Laboratory, Livermore, Calif., unpublished finite element code for linear static/dynamic thermoelastic/viscoelastic analysis of plane and axisymmetric solids (LLL Photostore User's Manual ELF RDS .328712:DYNA76:DTVIS2M).
6. J. O. Hallquist, NIKE2D--An Implicit, Finite Deformation, Finite Element Code for Analyzing the Static and Dynamics Response of 2-D Solids, Lawrence Livermore Laboratory, Livermore, Calif., UCRL-52678.
7. G. S. Holman and M. A. Gerhard, Calculation of Three-Dimensional Bubble Loads for the Mark I Hydro-Structure Interaction Analysis, Lawrence Livermore Laboratory, Livermore, Calif., UCID-18014 (December 1978).
8. W. H. McMaster, et al., Coupled Fluid-Structure Method for Pressure Suppression Analysis, Lawrence Livermore Laboratory, Livermore, Calif., UCRL-52620 (February 1979).
9. Working Group Meeting on Hydro-Structure Interaction (LLL, NRC, GE) at Livermore, Calif. (April 5, 1978).
10. C. M. Harris and C. E. Crede, Shock and Vibration Handbook, Vol. 1, (McGraw-Hill, New York, 1961).

11. H. T. Tang, Fluid-Structure Interaction Analysis of a Ramshead Safety Relief Value Discharge in a Mark I Steel Containment Torus, General Electric Co., NEDO-23834 (June 1978).

12. Presentation by Acurex Corp. of 1/12-scale FSI/chug experiments at Mountain View, Calif. (April 27, 1978).

FWB/jvb

APPENDIX

COMPUTER CODE DESCRIPTIONS

G. L. Goudreau
S. J. Sackett
(Methods Development Group,
Mechanical Engineering Department)

TWO-DIMENSIONAL LINEAR FINITE ELEMENT CODE DTVIS2

DTVIS2 is a two-dimensional plane or axisymmetric implicit finite element code.[1] It treats quasi-static or dynamic thermoviscoelastic behavior of solids. Its principal development is small deformation linear solids but has been extended to a limited class of nonlinear elastic materials.

For the purpose of the SRV discharge and LOCA chug calculations, the basic quadrilateral element was converted to a constant pressure fluid element which worked successfully. The small deformation assumption was adequate because the peak structural reactions occur before deformations become large. At late times the bubble continues to grow, obviating the small deformation condition and requiring both large deformation kinematics and follower pressure. Another implicit finite element code (NIKE2D) treating large deformations and follower pressure is available for solids.[2] This was modified to provide a fluid element too late to impact the LOCA analysis matrix of calculations for FY77. A benchmark calculation, however, showed the DTVIS2 results to be adequate. DTVIS2 was then used for the FY78 parameter study.

The spatial discretization for DTVIS2 is accomplished by use of quadrilateral four-node linear isoparametric elements. The usual equations of motion are obtained:

$$M\ddot{\underline{u}} + K\underline{u} = \underline{P}(t) \quad ,$$

with

$$M = \int_V \rho \Phi^T \Phi \, dv$$

$$K = \int_V B^T D B \, dv$$

$$\underline{P} = \int_{\underline{S}} \Phi^T \underline{t} \, ds \quad ,$$

with M, K, P the mass and stiffness matrices and load vector, ρ the density, D the elastic modulus matrix, t the prescribed surface traction vector, Φ the basis functions of the usual finite element displacement expansion, and B the matrix of the gradient of the basis functions. Integration is performed elementwise by appropriate Gauss quadrature:

$$D = kD_1 + \mu D_2 \quad ,$$

with k, μ the bulk and shear moduli and D_1, D_2 appropriate constant matrices.

Time integration is accomplished by the unconditionally stable Newmark scheme.[3]

The application of this element to Lagrangian fluid problems of the LOCA type leads to the use of a small trace shear modulus, μ, to stabilize the grid. The resulting large, nearly incompressible distortions are restricted by a locking of the elements due to excessive kinematic constraints on the element deformation. This results from the multipoint integration of the bulk stiffness.[4] However, one-point integration of the bulk stiffness with 2×2 integration of the trace shear stiffness overcomes this problem and results in a successful calculation.

DTVIS2 has an axisymmetric (or plane cylinder) thin-shell element using the cubic polynomial Grafton and Strome formulation.[8] However, the user defines the shell element as a quadrilateral in terms of its surface coordinates. The code internally computes the midsurface where the thin shell is formulated, and then those coordinates are transformed to the global surface coordinates. A penalty function is introduced to constrain the pinching of the shell through its thickness.

TWO-DIMENSIONAL NONLINEAR FINITE ELEMENT CODE NIKE2D

NIKE2D is an implicit, large deformation, large strain, finite element code for analyzing the response of two-dimensional axisymmetric and plane-strain solids.[3] A variety of loading conditions can be handled, including traction boundary conditions, displacement boundary conditions, concentrated nodal point loads, body force loads due to base accelerations, and body force loads due to spinning. Slidelines with interface friction are available. Elastic, orthotropic, elastic-plastic, soil and crushable foam, thermoelastic-plastic, and linear viscoelastic material models are implemented. Nearly incompressible behavior that arises in plasticity problems and elasticity problems with Poisson's ratio approaching 0.5 is accounted for in element formulation to preclude mesh lockups and the associated anomalous stress states. Variable node elements are used for the spatial discretization, and bandwidth minimization is optional. NIKE2D accepts the same mesh slideline definition required by other codes at LLL.

NIKE2D is based in part on previous work by Bathe et al.[9] and Key[10] and includes many recent developments such as a general slideline capability behavior.

An incremental formulation is used that is based on the Jaumann stress rate with a symmetric stiffness matrix and Newton iterations. In each iterate, the load vector and the stress divergence vector with Cauchy stress are evaluated over the current estimate of the deformed configuration with stress rotations handled in an explicit update identical to that employed in the DYNA codes.[11] Fluid and plasticity problems are modeled by constant dilatation elements. Slidelines along material interfaces are treated by penalty functions. The validity of the implicit formulation has been verified by test problems and comparisons with experiments.

NIKE2D does not have a true shell element at this time. However, the constant pressure eight-node quadrilateral element is used, and appears to work satisfactorily. In the hydro/structure interaction problem, it was used in conjuction with the four-node fluid element.

ADAPTATION AND EVALUATION OF LLL-SAP4 FOR THREE-DIMENSIONAL HYDRO/STRUCTURE INTERACTION CALCULATIONS

SAP4[5] is the LLL version of the SAPIV code developed at UC/Berkeley by Bathe, Wilson, and Peterson.[6] It is used for static and dynamic analysis of linear elastic structures by the finite element method. Systems can be modeled using beam, pipe, plate, and shell, and two- or three-dimensional solid elements.

For analysis of the SRV problem, the water is modeled using eight-node solid elements (three-dimensional bricks). Values for Young's modulus and Poisson's ratio are chosen such that the bulk modulus (k) has the correct value for water and the shear modulus (μ) has a value approximately six orders of magnitude less than k. The trace shear modulus is required to stabilize the grid and prevent "hourglass" distortions during the time integration. Time integration is accomplished by the Wilson θ method.[7] This is an unconditionally stable algorithm which yields good results when the frequency content is low.[3]

To prevent "locking" of the elements in this nearly incompressible problem, SAP4 was modified to split the bulk and shear terms in the stiffness matrix and integrate each one separately. Locking is caused by excessive kinematic constraints on the element deformation--a result of exact (multipoint) integration of the bulk stiffness.[4,8] By using one-point integration for the bulk terms and $2 \times 2 \times 2$ integration for the shear terms, incompressibility is satisfied as an average element property and the problem of locking is avoided.

The original mass lumping scheme used for the three-dimensional brick was also found to cause inaccuracy in the SRV calculations. This scheme was modified in SAP4 to distribute the nodal mass for each element according to the basis functions rather than equally as per SAPIV.

To provide verification of the applicability of SAP4 to fluid-structure problems, the two-dimensional DTVIS2 finite element mesh was expanded to three

dimensions and analyzed with SAP4. A three-element thickness was originally defined for the slab mesh, but this was reduced to a one-element layer after a comparison study indicated a one-element layer was sufficient for the plane-strain problem. Comparison between the two- and three-dimensional analyses (using D/t = 300) indicated excellent agreement in both nodal displacements (Fig. 14) and pressures (Fig. 15) predicted at the pool bottom. This agreement was consistently repeated between both models at other locations as well. Details of the comparison are given in the SRV section of this document headed "Three-Dimensional Investigations."

SAP4 uses the same thin-shell element as the original SAPIV. Its cubic polynomial bending formulation makes it the two-dimensional equivalent of the DTVIS2 Grafton-Strome element.

APPENDIX REFERENCES

1. G. L. Goudreau, DTVIS2 User's Manual, Lawrence Livermore Laboratory, Livermore, Calif., unpublished finite element code for linear static/dynamic thermoelastic/viscoelastic analysis of plane and axisymmetric solids (LLL Photostore User's Manual ELF RDS .328712:DYNA76:DTVIS2M).
2. J. O. Hallquist, NIKE2D--An Implicit, Finite Deformation, Finite Element Code for Analyzing the Static and Dynamics Response of 2-D Solids, Lawence Livermore Laboratory, Livermore, Calif.,UCRL-52678.
3. G. L. Goudreau and R. L. Taylor, "Evaluation of Numerical Integration Methods in Elastodynamics," Computer Methods in Applied Mechanics and Engineering, 2, 1 (1973).
4. D. S. Malkus and T. J. R. Hughes, "Mixed Finite Element Methods--Reduced and Selective Integration Techniques: A Unification of Concepts," Computer Methods in Applied Mechanics and Engineering, 15 (1978), pp. 63-81.
5. S. J. Sackett, SAP4 User's Manual, Lawrence Livermore Laboratory, Livermore, Calif. (document in preparation).
6. K. Bathe, E. L. Wilson, and F. E. Peterson, SAPIV--A Structural Analysis Program for Static and Dynamic Response of Linear Systems, University of California, Berkeley, Calif., EERC 73-11 (April 1974).
7. E. L. Wilson, A Computer Program for the Dynamic Stress Analysis of Underground Structures, University of California, Berkeley, Calif., SEL 68-1 (January 1968).
8. O. C. Zienkiewicz, The Finite Element Methods, 3rd ed. (McGraw-Hill, London, 1977), pp. 284-288.
9. K. J. Bathe, E. L. Wilson, and R. H. Iding, NONSAP--A Structural Analysis Program for Static and Dynamic Responses of Nonlinear Systems, University of California, Berkeley, Calif., UCSESM 74-3 (1974).
10. S. W. Key, HONDO--A Finite Element Computer Program for the Large Deformation Dynamic Response of Axisymmetric Solids, Sandia Laboratories. Albuquerque, N. M., 74-0039 (1974).
11. J. O. Hallquist, DYNA2D--An Explicit Finite Element and Finite Difference Code for Axisymmetric and Plane Strain Calculations (User's Guide), Lawrence Livermore Laboratory, Livermore, Calif., UCID-52429 (1978).

NRC FORM 335 (7-77)

U.S. NUCLEAR REGULATORY COMMISSION

BIBLIOGRAPHIC DATA SHEET

1. REPORT NUMBER (Assigned by DDC)
NUREG/CR-0746
UCRL-52624

TITLE AND SUBTITLE (Add Volume No., if appropriate)
The Effects of Torus Wall Flexibility on Forces in the Mark I Boiling Water Reactor Pressure Suppression System--Final Report.

2. (Leave blank)

3. RECIPIENT'S ACCESSION NO.

AUTHOR(S)
S.C. Lu, G.S. Holman, E.W. McCauley

5. DATE REPORT COMPLETED
MONTH: October | YEAR: 1978

PERFORMING ORGANIZATION NAME AND MAILING ADDRESS (Include Zip Code)
LLL/NRC
P.O. Box 808
Livermore, CA 94550

DATE REPORT ISSUED
MONTH | YEAR

6. (Leave blank)

8. (Leave blank)

12. SPONSORING ORGANIZATION NAME AND MAILING ADDRESS (Include Zip Code)
U.S. Nuclear Regulatory Commission
Engineering Branch
Office of Nuclear Reactor Regulation
Washington, D.C. 20555

10. PROJECT/TASK/WORK UNIT NO.

11. CONTRACT NO.
FIN A-0203

13. TYPE OF REPORT
Final Technical Report

PERIOD COVERED (Inclusive dates)

15. SUPPLEMENTARY NOTES

14. (Leave blank)

16. ABSTRACT (200 words or less)

This report summarizes the FY78 results of a program funded in FY77 and FY78. The purpose was to investigate, through analytical models, the effects of wall flexibility on hydrodynamically induced loads in the torus-shaped pressure suppression chamber of a Mark I boiling water reactor, both in the event of a safety relief valve (SRV) discharge and a hypothetical loss-of-coolant accident (LOCA). Two-dimensional and three-dimensional analytical models for these two events were created by using the Monticello nuclear plant's geometry and finite element computer codes. Initial two-dimensional results were documented in the FY77 report (Lawrence Livermore Laboratory, UCRL-52506); those two-dimensional results are extended here by varying the pulse amplitudes and conducting nonlinear analyses for comparison with the linear analyses. Finally, three-dimensional analyses are conducted for the SRV discharge and LOCA chug problems. Our analytical models show that, compared to rigid wall response, flexibility in the torus shell significantly decreases hydrodynamic loads in the suppression chamber.

17. KEY WORDS AND DOCUMENT ANALYSIS

17a. DESCRIPTORS

17b. IDENTIFIERS/OPEN-ENDED TERMS

18. AVAILABILITY STATEMENT
Unlimited

19. SECURITY CLASS (This report)
Unclassified

21. NO. OF PAGES

20. SECURITY CLASS (This page)
Unclassified

22. PRICE
$

NRC FORM 335 (7-77)